nature energy

Consensus Statement https://doi.org/10.1038/s41560-026-02101-x

Best practices for measuring the performance and stability of indoor photovoltaic devices

Received: 24 April 2025

Accepted: 30 April 2026

Published online: 18 August 2026

Check for updates

A list of authors and their affiliations appears at the end of the paper

Indoor photovoltaics harvests energy from light available inside homes and buildings for powering the Internet of Things, wireless sensors and consumer and medical electronics. A major challenge in this field is a lack of standardized testing conditions. Here a team from more than 60 research institutions and companies proposes best practices for evaluating indoor photovoltaic performance and establishing baseline stability tests. We base these recommendations on recent experimental data, published literature, practices used in academic and industrial settings, technical specifications from standards organizations, lighting databases and existing regulations. We outline procedures that begin with the recommendation of a single artificial light source, followed by guidance on setting up measurement systems and a step-by-step guide for conducting measurements and tests. These procedures are consolidated into three checklists. Our aim is to promote accurate measurement of laboratory and commercial solar cells and modules under indoor lighting, facilitating comparability across academia and industry worldwide.

Indoor photovoltaics (iPV) converts lighting present in buildings into usable electrical energy. Even though indoor irradiances (15–330 μW cm^{-2}) are low compared to sunlight (10^4–10^5 μW cm^{-2}), iPV has enormous potential as a sustainable battery-free power source. The theoretical power conversion efficiency (PCE) limit exceeds 50% under narrow spectral distribution of artificial light sources (compared to ~33% for solar cells under sunlight's much broader spectrum[1,2]). Amorphous silicon has been the dominant commercial iPV technology, delivering typical PCEs of 7–16%, with flexible geometrical design at the module level[3]. Next-generation technologies, including organic, perovskite, dye-sensitized and III-V semiconductors, have reached PCEs of 30–45% indoors at the small laboratory-cell level, driving strong academic and industrial interest[3,4]. Together, these advances position iPV as a viable pathway towards autonomous, sustainable power for the billions of internet of things (IoT) and wireless electronics devices in an increasingly connected 'smart' world[5,6].

Solar PV benefits from measurement norms (for example, International Electrotechnical Commission's (IEC) IEC 60904) and the globally accepted Standard Test Conditions (STC; 1,000 W m^{-2} irradiance, 25 °C temperature, AM1.5 G spectral irradiance)[7–10]. iPV lacks an equivalent widely-adopted universal standard, and the resulting variability in light sources, illumination conditions, equipment and procedures makes fair performance comparisons difficult, with inconsistencies even reaching 60% in relative terms[11–14]. Differences in spectral response and charge carrier recombination dynamics in cells mean that the power output of iPV devices is strongly dependent on both incident spectra and irradiance[13].

Research groups have started to tackle and provide solutions to these challenges, towards standardization[2,14–24]. In fact, international bodies emphasize early standardization as a catalyst for innovation and commercialization, substantially reducing time to market for new technologies[25–27].

In 2023, the IEC published Technical Specification (TS) IEC TS 62607-7-2:2023, establishing methodologies for measuring iPV efficiency[28], representing an important milestone. Nevertheless, key issues need addressing. As iPV devices operate under diverse spectra and irradiance, testing across all these varied conditions can be informative, yet time-consuming, and can hamper development of new materials and device solutions. Furthermore, the diversity in incident light spectra creates uncertainty over whether maximum power density (MPD) or PCE should be prioritized in reporting.

To fix the relationship between MPD and PCE, and to ensure consistent performance comparison and quality assurance across laboratories and manufacturers, this consensus statement puts forward a

e-mail: thomas.brown@uniroma2.it

https://doi.org/10.1038/s41560-026-02101-x

single reference spectrum and illuminance level as 'best practice' with general relevance, drawing on market and regulatory analyses. We also identify 'highly recommended' alternatives to the 'best practice' choice that cover lighting differences found in building environments. This tiered framework, extending to measurement systems and procedures including masking and calibration, balances practical constraints with rigorous performance assessment. Core assessment tests for stability of iPV devices are also introduced, addressing a critical gap in current performance evaluation. At the end of this consensus statement, we provide step-by-step best practice procedural guidelines in tabular form. Broad adoption of these practices will strengthen reproducibility, accelerate translation of iPV technologies to real-world deployment and establish a foundation for protocols and energy ratings standards that capture the diversity of indoor lighting and environmental conditions[2,14–24,29–33].

Selecting a light source for standardization

The IEC TS 62607-7-2 provides both a fluorescent (FL) and a light-emitting diode (LED) lamp spectrum as reference examples, while also allowing any user-defined 'U light' source. Given ongoing global legislation phasing out fluorescent lamps (Box 1 provides an overview of indoor lighting technologies and spectra), we recommend using phosphor-converted white LEDs (WLEDs) or hybrid red, green, blue and white (RGBW) WLEDs for iPV testing as their emissions profiles most closely match the WLED illuminants defined by the Commission Internationale de l'Éclairage (CIE). Of these, LED B-4 (5,000 K) was adopted by IEC TS 62607-7-2, reflecting the prevalence of 5,000-K sources in industrial lighting during 2014–2018[34,35], and is the current best practice.

Recommendation for a future best practice WLED reference

Over the past decade, the lighting market has evolved. To identify the best lighting spectrum with the widest applicability moving forward, we conducted a market study (Market Analysis in Methods). A distinct preference for 2,700 K warm WLEDs (Fig. 1a) in residential settings was found based on analyses of consumer LED products on Amazon.com (50.1%), GE Lighting's direct-to-consumer website (39.9%) and European market data from topten.eu (79.2%) (refs. 36–38). The non-residential sector exhibits an even clearer consensus (Fig. 1b), with 4,000 K lighting widely adopted by major suppliers, including Lithonia Lighting (25.6%), Signify (80%) and European commercial installations (83.3 %) (refs. 38–40). For indoor PV-powered IoT devices, the commercial sector represents the largest market opportunity as it consumes considerably more electricity for lighting compared to residential (168 versus 76 TWh yr^{-1} in the USA in 2024)[41]. Additionally, higher CCT LEDs (for example, 4,000 K) can offer superior energy efficiency compared to warmer sources.

Regulatory standards worldwide (Lighting Regulatory Analysis in Methods) show similar preference with residential spaces favouring 2,700 K and non-residential spaces favouring 4,000 K, reflecting their differing functional needs[42–47]. Crucially, after decades of using standard illuminant A (incandescent light), the CIE officially adopted the CIE reference spectrum L41, identical to LED B-3 (4,000 K) but tabulated from 360 to 830 nm rather than 380 to 780 nm, for calibrating photometers that measure illuminance[34,48], the same parameter required for iPV characterization.

We therefore advocate for CIE LED B-3 (4,000 K) becoming the future best practice reference for iPV performance evaluation and recommend its adoption in the forthcoming IEC technical specifications. This choice ensures strong market relevance, regulatory alignment and consistency with lighting industry standards, thereby supporting seamless translation of iPV technologies from research to commercial products.

Our detailed balance limit calculations[49] indicate that the maximum theoretical PCEs achievable by iPV devices under the five CIE

BOX 1

Overview of indoor lighting technology and spectra

A wide variety of artificial light sources illuminate indoor environments, including thermal sources (incandescent/halogen), discharge lamps such as fluorescent lamps (FLs) and solid-state devices such as LEDs[126]. Panel a shows that compared to the broad AM1.5 G spectrum (grey)[127], the most prevalent indoor sources, FL (FL-10 in green) and LEDs (LED B-3 in blue)[48], have spectra confined to the 380–780-nm visible range, closely aligned with the spectral luminous efficiency function $V(\lambda)$ (brown dashed line)[128], which describes the sensitivity of the human eye under photopic vision.

Since 2023, the European Union, the USA, China and 147 countries have enacted agreements or legislation to phase out fluorescent lamps[42,43,129,130], making LEDs the natural reference technology for iPV testing. WLEDs are primarily realized through blue LEDs coated with yellow-emitting phosphors, combining RGB LEDs or through hybrid RGBW architectures that integrate both strategies, expanding spectral coverage and allowing versatile spectral tuning[131].

A key metric for characterizing lighting is correlated colour temperature (CCT, in kelvin), which describes the perceived colour of a light source from warm yellowish (low CCT) to cool bluish (high CCT) tones[132–134]. CCT selection is typically tailored to the environment[135]: warm white (2,700–3,000 K) suits living and hospitality spaces; neutral white (3,500–4,000 K) in retail and offices; cool white (CCT ≥ 5,000 K) in task lighting and healthcare; daylight (CCT ≥ 6,500 K) in outdoor and security applications. The CIE[136] has defined five representative white LED illuminants, as shown in panel b[137], with CCTs of 2,700 K (LED B-1); 3,000 K (LED B-2); 4,000 K (LED B-3); 5,000 K (LED B-4) and 6,500 K (LED B-5), derived from spectral analyses of 1,516 commercial LED products[34].

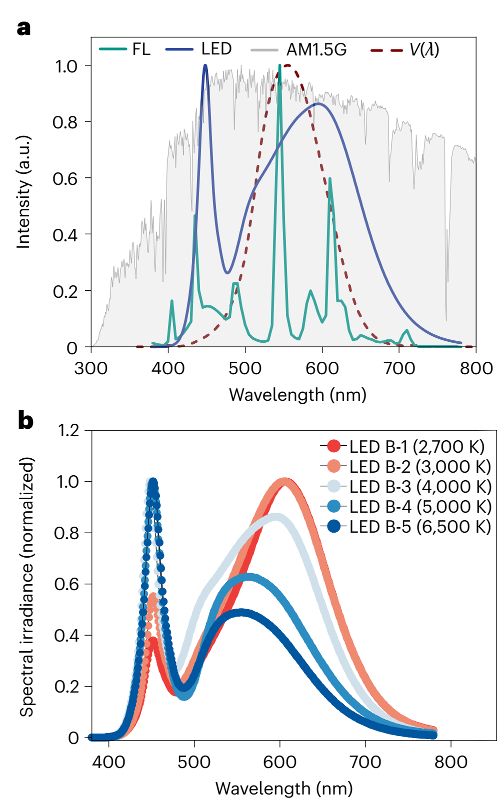

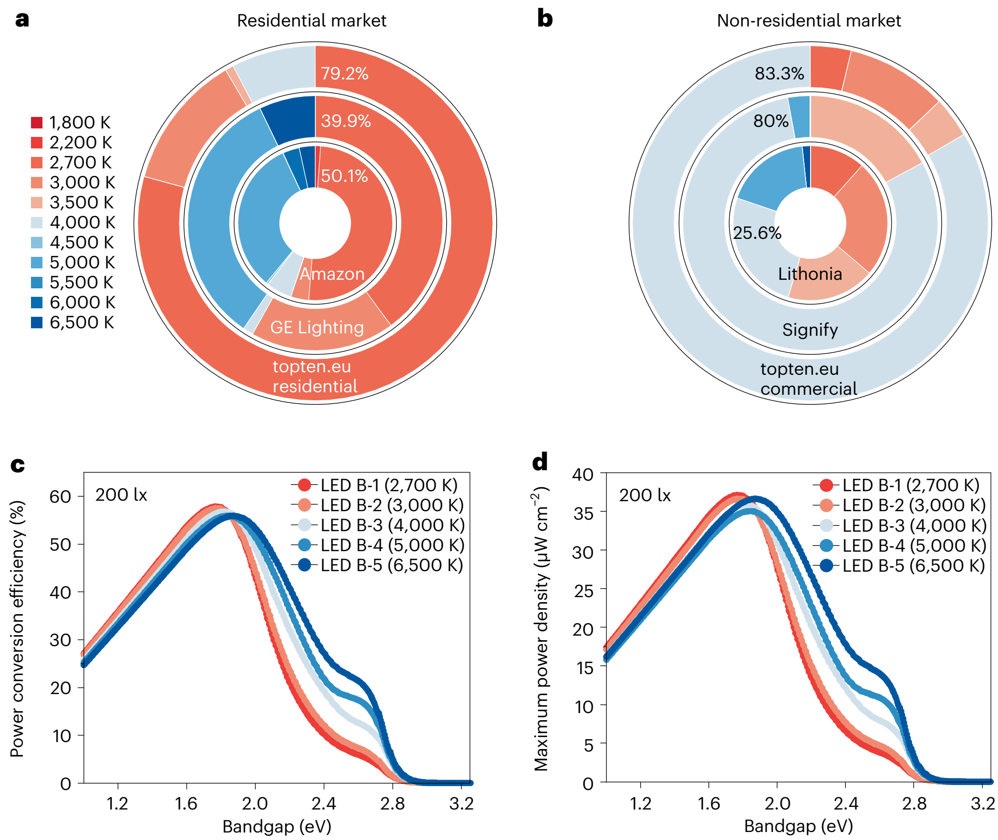

Fig. 1 | WLED market preferences and maximum efficiencies and power densities attainable from PV devices under WLED light. a, Analysis of residential LED products from Amazon.com consumer marketplace[36] (inner pie), GE Lighting's direct-to-consumer website[37] (middle pie) and best LED home luminaires based on 2023 European market data from topten.eu[38] (outer pie). **b**, Analysis of industrial LED product distribution from major suppliers, Lithonia Lighting[39] (inner pie) and Signify Lighting[40] (middle pie) and best office luminaires based on 2023 European market data from topten.eu[38] (outer pie). Each pie chart segment represents the proportion of light source products with a particular CCT, illustrating the prevalent colour temperature preferences across different market sectors. **c**,**d**, Detailed balance limit calculations of maximum power conversion efficiency (**c**) and maximum power density (**d**) at 200 lx of PV devices as a function of bandgap, obtainable under the five different CIE LED spectra, LED B-1, LED B-2, LED B-3, LED B-4 and LED B-5. The MPD and PCE are: 37.09 μW cm^{-2}, 57.84% for LED B-1, 2,700 K; 36.61μW cm^{-2}, 57.47% for LED B-2, 3,000 K; 35.80 μW cm^{-2}, 56.74% for LED B-3, 4,000 K; 35.00 μW cm^{-2}, 55.89% for LED B-4, 5,000 K; and 36.59 μW cm^{-2}, 55.85% for LED B-5, 6,500 K.

LED illuminants range from 55.9% to 57.8% (Fig. 1c), with corresponding MPDs between 35.0 and 37.1 μW cm^{-2} at 200 lx (Fig. 1d). Although slightly higher PCEs are calculated for the warmer lamps, theoretical efficacies in lumens per watt generally favour higher CCTs[50,51]. Importantly, the differences of MPDs and PCEs values under LED B-3 and LED B-4 fall within typical experimental uncertainties.

Whereas LED B-3 (future) or LED B-4 (current) should serve as the 'best practice' reference, researchers focusing on specific applications, such as devices intended for warm residential lighting, may adopt the 'highly recommended' approach using a lamp closely matching LED B-1 (2,700 K) spectrum (and to adopt LED B-1 as reference).

Illumination levels

In conventional photovoltaics, spectral irradiance, $E(\lambda)$ (W m^{-2} nm^{-1}) and total input irradiance, P_{in} (W m^{-2}), are used to characterize light incident on the device (that is, AM1.5 G and 1,000 W m^{-2} at STC), where

$$P_{in} = \int E(\lambda)\,d\lambda. \quad (1)$$

Because the interiors of buildings are designed for human occupancy, the relevant portion of the electromagnetic spectrum is the one that is perceivable by the eye. For this reason, engineers and regulators specify lighting requirements in photometric units, which are weighted by the spectral sensitivity of the human visual system, described by the photopic luminosity function $V(\lambda)$, which peaks at 555 nm and tails off rapidly beyond the ~400–700 nm range. The corresponding quantity to irradiance is illuminance, E_v, measured in lux:

$$E_v = K_m \times \int E(\lambda) \times V(\lambda)\,d\lambda, \quad (2)$$

where K_m is a scaling factor equal to 683 lm W^{-1} (ref. 52). Because the application of iPV is primarily within buildings where photometric units are mostly used, it has become customary to specify the illuminance of the incident light when evaluating performance, alongside irradiance (necessary to extract PCE). This approach ensures seamless integration of iPV systems into existing indoor lighting environments.

Indoor environments operate mostly between 100 and 1,000 lx, as defined by European standard EN 12464-1:2021[53], with most spaces falling within 200–500 lx (first nine bars of Fig. 2a). These standards prioritize human visual comfort in areas where people typically direct their gaze, such as office desks. Illuminance varies elsewhere depending on lighting design, room architecture and device placement, generally being dimmer away from windows[54]. The last bar ('Exp.OFC') in Fig. 2a illustrates that illuminance readings (Illuminance Measurement in the Methods) on desk surfaces without additional task lighting do match the 200–500 lx recommended levels. Wall-mounted positions, common for IoT devices, ranged from 60–200 lx depending on height, whereas ceiling ones measured the lowest at 30–50 lx. To account for

https://doi.org/10.1038/s41560-026-02101-x

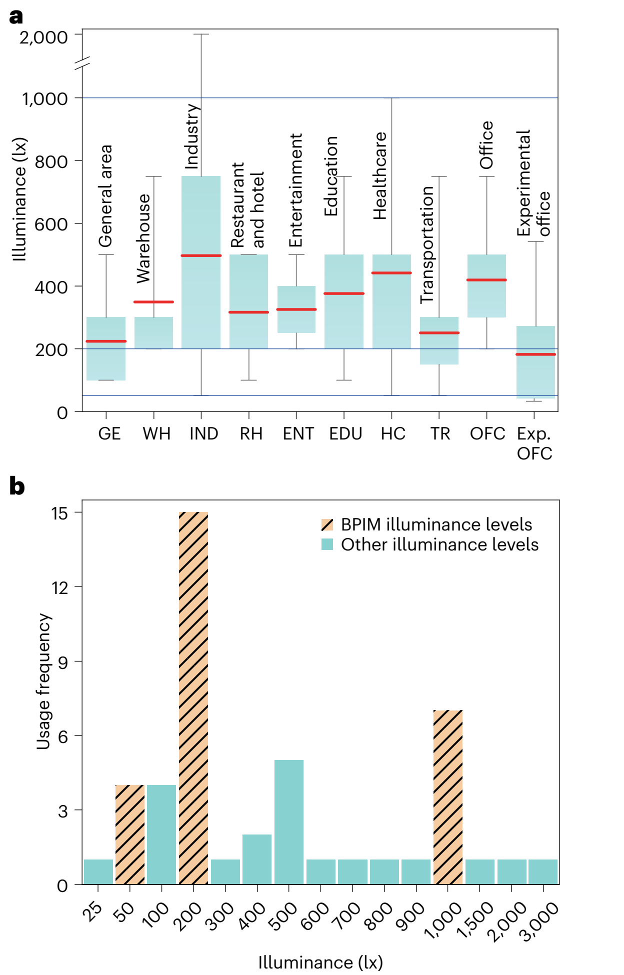

Fig. 2 | Illuminance levels found in indoor environments and used by commercial developers of PV. a, Illuminance levels as recommended by European Committee for Standardization[53] for various indoor locations: general area (GE), warehouse (WH), industry (IND), restaurant and hotel (RH), entertainment (ENT), educational facilities (EDU), healthcare (HC), transportation (TR) and office (OFC). The turquoise boxes represent the interquartile range (25th–75th percentile) of recommended values from lighting standards, whereas the black whiskers indicate the minimum and maximum recommended values. Red horizontal lines within boxes show mean values. A *y*-axis break is introduced between 1,000 and 2,000 lx to display higher values without compressing the lower, more commonly used illuminance range. The blue horizontal lines at 50 lx, 200 lx and 1,000 lx represent the best practices for indoor photovoltaic measurement (BPIM) illuminance levels. The final box in the 'experimental office' (Exp.OFC) section represents the illuminance measured at various positions in the Tor Vergata University of Rome office, across desks, walls and ceiling (no sunlight entered the room and the luxmeter sensor was planar to the surfaces). **b**, Histogram with distribution of illuminance levels used by 15 commercial companies focusing on PV products for indoors when reporting PV performance under indoor illumination. The counts at the 50-lx, 200-lx and 1,000-lx levels are highlighted in hatched yellow bars. The usage frequency indicates how many companies use each illuminance level in the datasheets/reports found on their websites for their indoor PV devices[55–69]. Note that 200 lx is the only illuminance level at which all 15 companies provide performance of their PV devices.

this variability, the IEC technical specification recommends testing at three illuminance levels: 50, 200 and 1,000 lx.

Although comprehensive characterization at all three illuminance levels is ideal, this can be impractical for laboratories processing hundreds of samples weekly or conducting long-term stability tests requiring frequent measurements. As best practice, we identify 200 lx as the primary illuminance at which iPV performance must always be reported, as it represents typical indoor environments (Fig. 2a), is unanimously adopted by all major commercial indoor PV manufacturers[55–69] (Fig. 2b) and provides a practical compromise between bright and dim environments.

To facilitate reporting, we introduce the general label BPIM-B#-#lx. As an example, 'BPIM-B3-200lx' signifies performance has been evaluated at the best practices for indoor photovoltaic measurement (BPIM) conditions of 200 lx under LED B-3 (future best practice) incident light. For best-performing or representative devices tested at 200 lx, we 'highly recommend' additional measurements at 1,000 lx (BPIM-B3-1000lx), representative of bright commercial environments such as supermarkets (the second-most reported commercial value in Fig. 2b) and at 50 lx (BPIM-B3-50lx), representing dim conditions that will become increasingly relevant as the indoor PV market expands. If another LED is used instead of LED B-3, the corresponding 'B#' designation should be applied (for example, B4 for LED B-4). This tiered approach balances practical testing constraints with comprehensive characterization of device performance.

iPV measurement system

Test chamber design

In its basic configuration, the iPV measurement set-up comprises of (Fig. 3a,b): a light-tight enclosure with matte black interior and optional baffle plates to minimize stray light; a co-planar sample stage capable of accommodating the device under test (DUT), a photometer/reference cell, so that they all receive the same light intensity, and temperature sensors; a light source (LED lamp or array); a source measure unit with high-sensitivity (currents to be reported could be well below μA range for small lab cells) with software for I–V characterization including variable scan rates, directions and delay times.

A key design decision concerns the directionality of light beams, as collimated light, where rays travel normal to the DUT plane, offers better spatial uniformity and more predictable errors[2,20,70], whereas diffuse light better mimics realistic indoor conditions in which light scatters from multiple directions. We recommend using pseudo-collimated light sources to improve consistency[14]. For non-collimated light sources, we recommend applying sufficient distance between source and DUT, low-reflectance (< 3–5%) black coatings to the inner surfaces of the chamber (including behind the DUT when measuring semi-transparent or bifacial devices) or baffles to suppress reflections[71]. For LED arrays, uniform irradiance should be achieved through proper system design rather than by adding diffusers[72].

Intensity of light incident on the DUT can be controlled via three different illuminance adjustment systems (IAS): power control (IAS-P), optical attenuation (IAS-O) and distance adjustment (IAS-D), each with distinct advantages and limitations. IAS-P modulates the amplitude of the current driving the LED. This represents the preferred method[18], although the emission spectra of LEDs can change with driving current, and some LEDs may not operate reliably at very low or high currents. Instead, IAS-O uses optical media such as neutral density (ND) filters or prism attenuators[18] to reduce light intensity. This method can also introduce spectral changes as light passes through the optical elements. A variant employs micromirror arrays that adjust the number of mirrors directing light towards the device, offering precise intensity control with minimal spectral dispersion when combined with stray-light-blocking baffles[73]. Finally, IAS-D modulates the intensity by varying the space between the DUT and the light source. It offers simplicity and consistent spectra but presents challenges in maintaining spatial uniformity, particularly when positioning the light source close to the DUT at higher illuminance levels, where irradiance inaccuracies can become very large[20]. Unless optics are used, distances should be kept at the tens (≥ 30) of centimetres at minimum. Comparative studies have shown efficiency measurement ambiguities of approximately 2% with IAS-P and 6–15% with IAS-O methods[18]. As a general

https://doi.org/10.1038/s41560-026-02101-x

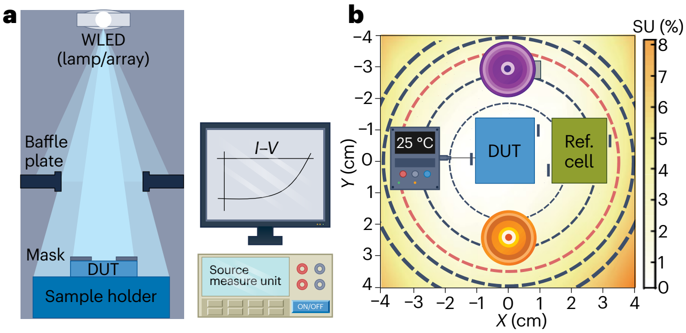

c

Class	SA	A	B	C
SC	0.95–1.05	0.75–1.25	0.6–1.4	0.4–2.0
SU	Within ± 2%	Within ± 2%	Within ± 5%	Within ± 10%
TS	Within ± 0.5%	Within ± 0.5%	Within ± 2%	Within ± 10%

Fig. 3 | Experimental set-up for indoor photovoltaic measurements under white LED illumination. a, Schematic of the light-tight measurement system with white LED (WLED) lamp or LED array, baffle plate, mask, DUT and sample holder (left) and source measure unit and computers that enables current–voltage (*I*–*V*) characterization and real-time display of electrical data on a screen (right). **b**, Schematic diagram of a DUT plane showing spatial non-uniformity (SU) of the incident light. Note that the DUT (blue), reference cell (green), luxmeter (orange) and spectroradiometer (purple) have been placed in the zone with SU ≤ 2%, marked by a red dashed line, corresponding to class SA/A of the measurement system in the spatial uniformity category. **c**, Classification of iPV measurement systems based on spectral coincidence (SC), spatial non-uniformity (SU) and temporal stability (TS) requirements (data from ref. 28). The four accuracy classes (SA, A, B, C) are determined by the combination of these three parameters.

recommendation, spectral deviations must be documented in cases where they are substantial.

Classification of indoor light systems

Just as solar simulators are rated (IEC 60904-9[74]), iPV test systems also need standardized classifications to ensure not only reliable, comparable results across laboratories but also to help researchers and manufacturers assess the accuracy of the measurements obtained. Figure 3c illustrates the four-tier classification of indoor light systems, SA, A, B and C, applied to three performance categories[28]: spectral coincidence (SC); temporal stability (TS); spatial non-uniformity (SU). SA and A represent the highest and C the lowest class.

SC defines how well the incident irradiance spectrum matches the reference one by quantifying spectral mismatches between the two. For iPV, best practice is to obtain the lowest spectral mismatch between measured, $E(\lambda)$, and reference, $E_{ref}(\lambda)$ irradiance spectra, evaluated with spectral responsivity profiles $S_k(\lambda)$ ($K = 1, \ldots, 5$) of five simulated PV devices (bandgaps 2.4–1.12 eV) tabulated in IEC TS 62607-7-2 (ref. 28):

$$\mathrm{SC_a} = \frac{\int E(\lambda) S_k(\lambda)\,\mathrm{d}\lambda}{\int E_{\mathrm{ref}}(\lambda) S_k(\lambda)\,\mathrm{d}\lambda} \quad (3)$$

When the five simulated $S_k(\lambda)$ data are not available, SC can be simplified to (highly recommended):

$$\mathrm{SC_b} = \frac{\int E(\lambda)\,\mathrm{d}\lambda}{\int E_{\mathrm{ref}}(\lambda)\,\mathrm{d}\lambda} \quad (4)$$

and should be reported for all these four ranges: 360–510 nm, 510–570 nm, 570–620 nm and 620–830 nm. These wavelength intervals were chosen so that the power delivered by the lamps is evenly divided among all four intervals, that is, (25.0 ± 0.7)% for LED B-3 and (25 ± 5)% for LED B-4. This is a highly recommended simple method that can be adopted by all.

The above methods are meant to quantify SC related to a test system designed for measuring any type of device. However, if the DUT's spectral response or bandgap is known, the SC value can be determined accurately (though for that specific device only) using equation (5) (highly recommended), if the spectral response (S_D) or external quantum efficiency (EQE) of the DUT are available, or equation (6), if EQE, S_D and $S_k(\lambda)$ are not available but the energy gap of the PV device is known.

$$\mathrm{SC_c} = \frac{\int E(\lambda) \times \mathrm{EQE}(\lambda) \times (\lambda/hc)\mathrm{d}\lambda}{\int E_{\mathrm{ref}}(\lambda) \times \mathrm{EQE}(\lambda) \times (\lambda/hc)\mathrm{d}\lambda} \text{ or } \frac{\int E(\lambda) S_D(\lambda)\,\mathrm{d}\lambda}{\int E_{\mathrm{ref}}(\lambda) S_D(\lambda)\,\mathrm{d}\lambda} \quad (5)$$

$$\mathrm{SC_d} = \frac{\int E(\lambda)\,\mathrm{d}\lambda}{\int E_{\mathrm{ref}}(\lambda)\,\mathrm{d}\lambda} \quad (6)$$

where the upper bound of the integral in equation (6) is set to the absorption onset.

It must be noted that for selecting the limits of the integrals, reference LED B-3 is tabulated in its L41 form from 360 to 830 nm; all the others are from 380 to 780 nm.

TS defines how consistently the lamp maintains its irradiance over the measurement period. TS can be determined by monitoring the illuminance (or photocurrent) over time using a photometer (or photodiode) and is calculated as[28]:

$$\mathrm{TS} = \frac{E_{v,\max} - E_{v,\min}}{E_{v,\max} + E_{v,\min}} \text{ or } \frac{I_{\max} - I_{\min}}{I_{\max} + I_{\min}} \quad (7)$$

where $E_{v,max}$ (I_{max}) and $E_{v,min}$ (I_{min}) are the maximum and minimum illuminance (photocurrent) fluctuations recorded after stabilization of the LS.

SU defines how evenly the light spreads across the measurement area:

$$\mathrm{SU} = \frac{E_{v,\max} - E_{v,\min}}{E_{v,\max} + E_{v,\min}} \text{ or } \frac{I_{\max} - I_{\min}}{I_{\max} + I_{\min}} \quad (8)$$

where illuminance (or photocurrent) is measured either over the DUT or the full illumination area. At least 17 data points are required to verify homogeneity[28].

To achieve higher classification, we recommend selecting a WLED with a spectrum as close as possible to the reference spectrum, for example, LED B-3. iPV measurements should begin only after a stabilization time has elapsed, as many commercial LED lamps need at least 30 minutes to reach stable operation[16,20]. Additionally, to improve SU (Fig. 3b), use pseudo-collimated light sources when possible. In the case of a non-collimated light source, uniformity can be improved by increasing the distance between the LS and the DUT and suppressing stray lights using baffle plates and masks. For maintaining stable light output (TS and SU), use active cooling of the light source (for example, water plates, heat sinks or fans).

Calibration of illuminance and input irradiance at DUT

Accurate indoor PV measurements require precise control and measurement of the illuminance (E_v) and input irradiance (P_{in}) of light incident on the DUT. Three primary methods can be used depending on the required accuracy and budget. Each takes their name from the equipment used for calibration: reference cell, spectroradiometer or luxmeter.

Reference cells, here representing best practice, consist of a highly stable photovoltaic device, with known irradiance spectral responsivity, $S_{RC}(\lambda)$, in amperes per watt per square metre (A m^2 W^{-1}), often matched to the DUT's spectral and angular response. They are used to set E_v and P_{in} in the plane of measurement, thereby reducing errors from spectral, temperature and angular mismatches[20,75]. To account for the differences between the incident and reference light spectra, and for those in the spectral response between the DUT and reference cell, a correction value, the mismatch factor M, is implemented to ensure accurate determination of DUT performance.

The calibration procedure begins by measuring the reference cell current (I_{sc_RL}) under the user's measurement set-up illumination, with irradiance $E(\lambda)$:

$$I_{sc\_RL} = \int S_{RC}(\lambda) \times E(\lambda)\, d\lambda \quad (9)$$

and is brought to be equal to the current (I_{sc_RR}) the device would deliver under the reference spectrum $E_{ref}(\lambda)$ (for example, that of LED B-3 that delivers 200 lx illuminance), calculated as:

$$I_{sc\_RR} = \int S_{RC}(\lambda) \times E_{ref}(\lambda)\, d\lambda, \quad (10)$$

This procedure is accurate if $E(\lambda) = E_{ref}(\lambda)$, however, because the two rarely match, a mismatch factor M must be calculated to account for differences between the relative spectral responsivity of the reference cell, $S_{RC}(\lambda)$, and that of the DUT, $S_D(\lambda)$ (A W^{-1}) (ref. 15):

$$M = \frac{I_{sc\_RR} \times I_{sc\_DL}}{I_{sc\_RL} \times I_{sc\_DR}} \quad (11)$$

where I_{sc_DR} and I_{sc_DL} are the short-circuit currents of the DUT under reference and measured spectra, respectively, and calculated as:

$$I_{sc\_DR} = A \times \int S_D(\lambda) \times E_{ref}(\lambda)\, d\lambda \quad (12)$$

$$I_{sc\_DL} = A \times \int S_D(\lambda) \times E(\lambda)\, d\lambda. \quad (13)$$

The integral limits must cover the wavelength range of the irradiance spectrum $E(\lambda)$ or $E_{ref}(\lambda)$. One can replace S_D with EQE when the latter is the data available for the DUT through:

$$S_D(\lambda) = \mathrm{EQE}_D(\lambda) \times \frac{e\lambda}{hc} \quad (14)$$

For accurate measurement of $S_D(\lambda)$ or EQEs, readers should refer to refs. 76–78. IEC standards specify the differential spectral responsivity as the preferred method, with four simplified alternatives also provided[76].

Once M is calculated, the illuminance at DUT can be set by adjusting the current of the reference cell, such that:

$$I_{sc\_RL} = I_{sc\_RR}/M \quad (15)$$

Although this calibration approach works even with large mismatches[79], it is always best to source a light and a reference cell that closely matches the reference spectrum and the spectral responsivity of the DUT (for example, by using similar but stable semiconductors or filters), respectively. Where incident light is non (quasi) collimated, sourcing reference cells with similar angular responses to DUTs is beneficial[70].

Spectroradiometers, considered here highly recommended, deliver complete spectral irradiance $E(\lambda)$ curves. The resulting data enable direct calculation of E_v and P_{in} and gauging how well $E(\lambda)$ matches that of the reference. When using a spectroradiometer, the calibration begins with calculating I_{sc_DR} and I_{sc_DL} (equations (12) and (13)) and adjusting the intensity of the light incident on the DUT such that,

$$I_{sc\_DL} = I_{sc\_DR}. \quad (16)$$

It must be noted that spectroradiometers involve a higher initial cost and can be bought with calibration equipment. Appropriate versions are those that fit cosine collectors with planar surfaces (that is, resembling those of PV cells). Note that background drift at low illuminance (for example, 50 lx) can cause measurement errors of 20–142% (ref. 20), highlighting the need to take fresh background measurements instead of relying on a single initial reading.

Finally, luxmeters are portable illuminance meters often chosen for their affordability and portability. Although simple to use, they present several limitations[20]. Past commercial general-purpose luxmeters have been calibrated to CIE standard illuminant A (incandescent lamp), leading to spectral mismatch errors. Figure 4a shows the illuminance readings of a spectroradiometer with calibration certificate and four different commercial luxmeters at the same position under WLED at 200 lx. The first luxmeter, sourced with a valid calibration certificate traceable to National Institute of Standards and Technology (NIST), gave a reading within 5% of the calibrated spectroradiometer. Discrepancies of even 25% were found using non-calibrated equipment. Luxmeters are also suboptimal under diffuse light, because spherical diffusers capture light differently than the planar surfaces of PV devices, leading to angular mismatch effects[16].

Our overall recommendations are to use instruments calibrated and traceable to a National Metrology Institute (NMI)[80]. Under diffuse light, reference cells with stable spectral responsivities such as the DUTs are preferred over spectroradiometers and luxmeters because their planar geometry and angular response more closely match that of the DUT, resulting in more representative measurements. For routine illuminance setting, luxmeters can be used but must be calibrated (NMI-traceable) to WLED illuminant. All methods require knowledge of the absolute spectral irradiance $E(\lambda)$ to determine the PCE of the devices. $E(\lambda)$ should ideally be measured using a calibrated spectroradiometer and graphed in the report. When only relative spectral irradiance, $E_{rel}(\lambda)$, is available, the absolute spectral irradiance can be calculated knowing the absolute illuminance:

$$E(\lambda) = E_{rel}(\lambda) \times \left[E_v / \int E_{rel}(\lambda) \times V(\lambda) \times K_m d\lambda\right]. \quad (17)$$

During calibration of the test system and setting of the illuminance level, the measured P_{in} value of the light incident at the DUT plane, should agree with the theoretical values, $P^T{}_{in}$, that are provided in Box 2 for the standard LED illuminant most similar to the one used in the experimental test system. Discrepancies should be within ±5–10% (±10–20%) for the higher (lower) classes of the measurement system (Fig. 3c). If not, instrumentation may need to be re-calibrated. $P^T{}_{in}$ values from Box 2 also enable the determination of the conversion factor between PCE and MPD so that knowing one, the other can be readily calculated.

Masking of the DUT

Accurate measurements require careful definition of the area of the photovoltaic device[81]. Whereas certification standards typically demand large-area devices (≥1 cm^2), smaller cells (<1 cm^2) are often fabricated in research for throughput and material savings. These small-area devices are particularly susceptible to stray light and edge effects under non-collimated lighting[16,82,83], which can lead to an overestimation of the measured short-circuit current density (J_{SC}) compared to EQE-derived short circuit current density (J_{cal})[84] (Box 3 provides details on J_{cal}). Black opaque masks (Fig. 4b) provide an effective solution

https://doi.org/10.1038/s41560-026-02101-x

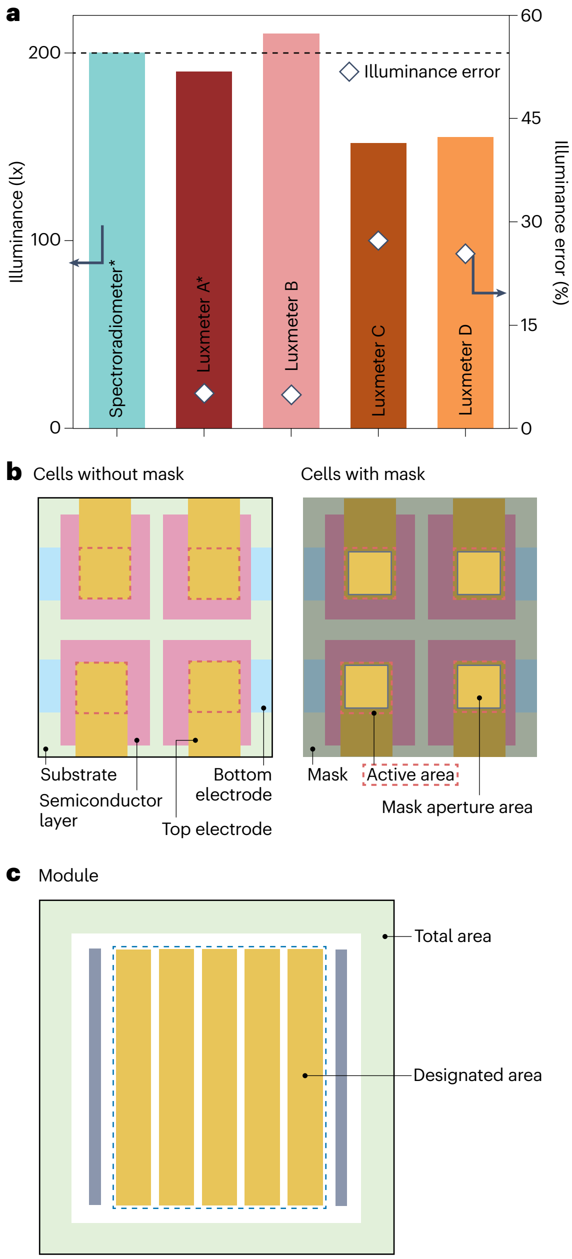

Fig. 4 | Best practices for calibration of illuminance and masking of DUT. **a**, Illuminance measurements (left axis) comparing that of a spectroradiometer with NMI-traceable calibration and Luxmeter A with NMI-traceable calibration certificate (both shown with a star sign), versus luxmeters B, C and D with no calibration certificates, demonstrating measurement variability under nominally identical 200-lx conditions. Diamond symbols indicate illuminance error relative to the spectroradiometer reference reading (right axis). **b**, Definition of active area and mask aperture area for small-area thin film laboratory photovoltaic cells. Preferably, the mask aperture area (yellow area with black solid line contour) should be 75–80% of the active area (yellow area with red dashed line contour). **c**, Definition of the areas for photovoltaic modules: total area (black solid perimeter line) and designated area (blue dashed line).

BOX 2

Theoretical irradiance under CIE LED spectra and MPD versus PCE conversion factor

The table below provides the theoretical incident input irradiances (P^{T}_{in}) calculated from spectral irradiance data for CIE illuminants LED B-1, LED B-2, LED B-3, LED B-4 and LED B-5 in the 380–780-nm range corresponding to illuminances of 1,000 lx, 200 lx and 50 lx (ref. 137).

Illuminance	1,000 lx	200 lx	50 lx
CCT (K)	P^{T}_{in} (μW cm^{-2})		
2,700 (LED B-1)	320.7	64.1	16.0
3,000 (LED B-2)	318.6	63.7	15.9
4,000 (LED B-3)	315.5	63.1	15.8
5,000 (LED B-4)	313.2	62.6	15.7
6,500 (LED B-5)	327.6	65.5	16.4

The PCE, a calculated parameter, is obtained by dividing the measured MPD, delivered by the PV device, by the P^{T}_{in} value corresponding to the light source used (for example, LED B-3) at one of the lux levels listed in the table (when P_{in} is not available experimentally).

PCE (calculated) = MPD (measured)/P_{in} (measured or tabulated)

Conversely, when only efficiency is given for an iPV device in a report, MPD can be estimated from the equation above. For example, an iPV device with an efficiency of 25% under LED B-3 at 1,000 lx ($P_{in} = P^{T}_{in}$ taken from the table above) will have a MPD = 0.25 × 315.5 = 78.88 (μW cm^{-2}).

By suggesting as best practice one light source that will be commonly used by all laboratories, with a spectrum as close as possible to the reference (for example, LED B-3), the relation between MPD and PCE is fixed (making MPD and PCE interchangeable, which is not the case when different light sources are routinely used).

to these measurement artefacts and represent the best practice for accurate performance characterization[85]. At 500 lx, using a 7.12-mm^2 aperture mask reduced J_{SC} overestimation from 10% to 7.8% compared with unmasked 9.80 mm^2 organic solar cells. The difference was lower (4% unmasked versus 3.7% masked) for 1-cm^2 cells[16]. Discrepancies can become larger under non-collimated light: at 1,000 lx, with an LED lamp positioned close to the DUT, masking reduced the J_{SC} overestimation in perovskite solar cells from 39% (4 × 4 mm^2 unmasked device) to 5% (3.5 × 3.5 mm^2 mask aperture) (Masking in Methods).

Whereas the mask aperture shape (circular versus square) has minimal impact, its area strongly influences PV parameters[86]. Apertures equal to the device active area make precise alignment impractical, leading to substantial measurement errors[83], whereas excessively small apertures cause J_{SC} overestimation and open circuit voltage (V_{OC}) underestimation due to enhanced edge effects[85,86]. Masks with apertures moderately smaller than the active area represent the optimal balance, minimizing stray light and edge effect, while maintaining acceptable V_{OC} accuracy. Therefore, as a good practice for indoor measurements, we recommend active areas of at least 1 cm^2 wherever possible, with smaller devices masked using precision-fabricated opaque black masks whose aperture area covers approximately 75–80% of the DUT area. Additionally, for lab-scale devices with multiple cells on the same substrate, it is best to avoid shared electrodes and ensure proper metallization of the contact areas to minimize contact resistance and electrical interference[87]. When defining areas for calculation and reporting of PV parameters, use the aperture area of the mask where present (report it together with the nominal area of the device in the experimental section). For PV modules, performance should be reported per designated area (Fig. 4c).

 https://doi.org/10.1038/s41560-026-02101-x

BOX 3

Validation of measured versus theoretical current density

The validation process compares the measured J_{SC} against a calculated theoretical value (J_{cal}) derived from integrating the EQE of the DUT with photon flux, $\Phi(\lambda)$[90], incident on it:

$$J_{cal} = e \times \int \Phi(\lambda) \times \mathrm{EQE}(\lambda)\, d\lambda$$

where

$$\Phi(\lambda) = E(\lambda) \times \lambda / \mathrm{hc},$$

and $E(\lambda)$ is the irradiance of the real light source at the selected illuminance, for example, 200 lx.

Acceptable discrepancies between J_{cal} and J_{SC} depend on the class of both the measurement system (each descriptor can vary by as much as ± 0.5–2% for class A to 10% for class C) and that of the EQE system. Standard tolerances can be 15–20% for lower-class systems and ≤10% for well-designed, more accurate systems[90,91].

For very high-performance devices (EQE~90%), one must also ensure:

$$J_{SC} - J_{cal} < e \times \int_{\lambda<\lambda_g}^{\lambda_g} \Phi(\lambda) \times (1 - \mathrm{EQE}(\lambda))\, d\lambda,$$

where the integral is calculated up to the wavelength λ_g that corresponds to the photovoltaic device bandgap[138,139]. This constraint ensures J_{SC} remains within the detailed balance efficiency limit (where EQE=1 above the bandgap). If the equation above is not respected, such as J_{SC} exceeding J_{cal} by 20% for a 90% EQE device, that will lead to unphysical results.

When EQE is not available, the table below can be used to verify if the results are physically reasonable. It provides theoretical maximum current densities (J_{cal_max}) for ideal devices (100% EQE) with common bandgaps of 1.12 eV (c-Si), 1.70 eV (a-Si:H), 1.90 eV (best E_g for LED B-3) and 2.10 eV (above the optimum, when photocurrents decrease rapidly) under the five CIE white LED illuminants. Measured J_{SC} values exceeding the theoretical J_{cal_max} limits reported in the table clearly flag serious measurement errors, often caused by incorrect illumination settings, and therefore require system recalibration.

	lux	1,000 lx				200 lx				50 lx			
	E_g	1.12 eV	1.70 eV	1.90 eV	2.1 eV	1.12 eV	1.70 eV	1.90 eV	2.1 eV	1.12 eV	1.70 eV	1.90 eV	2.1 eV
	Theoretical maximum current density limits, J_{cal_max} (μA cm^{-2})												
LED Type	LED B-1	153.0	149.4	120.6	62.03	30.60	29.87	24.14	12.40	7.652	7.468	6.035	3.101
	LED B-2	150.6	147.2	120.5	66.01	30.11	29.44	24.11	13.20	7.528	7.360	6.027	3.300
	LED B-3	143.5	141.5	123.3	79.73	28.69	28.30	24.67	15.94	7.173	7.074	6.168	3.986
	LED B-4	139.7	137.5	122.6	87.19	27.94	27.50	24.53	17.44	6.985	6.874	6.134	4.359
	LED B-5	142.8	141.2	129.3	97.91	28.56	28.24	25.87	19.58	7.141	7.059	6.468	4.895

Best practices for current–voltage (I–V) measurements under indoor light

This section outlines best practices for accurate current–voltage (I–V) measurement, photovoltaic parameter extraction, and standardized reporting to facilitate inter-laboratory and cross-technology comparison.

Before conducting I–V measurements, the illuminance (for example, 200 lx) must be set within ±5% of the desired level with good temporal stability ≤2% (ref. 28). The DUT temperature must be 25 °C ± 1 °C (ref. 28) and the DUT and the calibration device must be positioned co-planar within ±1 mm to minimize vertical variations in irradiance. I–V scans must be performed with sufficient data points to capture the complete curve shape, with PV parameters extracted from the I–V curves following IEC 60904-1:2020[10] and International Summit on Organic PV Stability (ISOS)[88] protocols. Specifically, linear interpolation must be used for extracting short-circuit current (I_{SC}), linear or low-order polynomial for V_{OC} and higher-order (≥ 4) polynomial for maximum power (P_{max}).

For stable devices, according to IEC TR 63228[89], the differences in P_{max} in the forward and reverse sweep directions, and over time (that is, across five different measurements), need to be less than 2% in relative terms:

$$\left(\frac{\Delta P_{max}}{P_{max\_avg}}\right) \times 100 \leq 2\%, \quad (18)$$

If equation (18) exceeds 2% or hysteresis is apparent, either report the actual values for equation (18) and/or both forward and reverse I–V scans (or associated PV parameters), or sample P_{max} continuously for 60–300 s, depending on technology. Reporting this 'stabilized' P_{max} (or PCE) avoids some of the artefacts and hysteresis that can arise from parameters used in voltage sweeps (just for the most representative or best-performing sample)[90–92]. For PV technologies such as dye-sensitized solar cells with high internal capacitances, fixing the voltage at V_{mpp} (voltage at maximum power point) and monitoring the current will suffice. Maximum power point tracking must be used if the maximum power point changes during the test period, with measurement delays, voltage steps, sweep times and 'Perturb and Observe' algorithms documented for better inter-laboratory comparison[93–95].

When reporting performance for modules (or large cells), provide not only I–V curves but also power–voltage (P–V) curves as well as I_{SC}, and P_{max}. Reporting also V_{mpp} can help to gauge electrical compatibility for integration with circuit elements in a product[31,96,97]. For small laboratory cells, provide the current density–voltage (J–V) curves and report J_{SC} instead ($J_{SC} = I_{SC} / A$, where A is the mask aperture area). For all devices, report also V_{OC}, fill factor (FF), MPD = P_{max_avg} / Area (where Area is defined by the mask aperture for laboratory cells and the designated area for modules and large cells) and PCE = MPD / P_{in}. For statistical analysis, provide average, standard deviation and experimental errors for all PV parameters. Single-device results should supplement, not replace, statistical data.

For devices approaching record performance (within 20% of published benchmarks at the time of publication), validation of the measured J_{SC} against calculated (J_{cal}) is required, especially for the purpose of academic publication. This validation step serves to identify calibration

 https://doi.org/10.1038/s41560-026-02101-x

discrepancies before publication, thereby ensuring the scientific rigour and defensibility of the results (Box 3).

Ancillary analysis of I–V curves for research purposes

In academic research, supplementary measurements using the basic equipment of the light source and source measure unit (SMU) to evaluate cell quality and predict its behaviour can be useful. Under dim light, the influence of shunt current becomes greatly amplified due to small photocurrents[98–100]. In the simplified single-diode model of a solar cell[101,102]

$$I = I_{\mathrm{ph}} - I_0\left[\exp\left(\frac{q(V+R_{\mathrm{s}}I)}{nkT}\right)-1\right]-\frac{V+R_{\mathrm{s}}I}{R_{\mathrm{sh}}}, \quad (19)$$

I is the net output current, I_{ph} and I_{o} are the photocurrent and dark saturation currents, R_{sh} and R_{s} are the shunt and series resistances. Under low illuminance, I_{ph} values are small. Thus, with typical resistance values found in cells, the effect of R_{sh} can become pronounced, diminishing fill factors and voltages. For example, with $R_{\mathrm{sh}} \leq 10^5\ \Omega\ \mathrm{cm}^2$, an 80% drop in cell efficiency can result when decreasing incident illuminance from 500 lx to 50 lx (refs. 17,103). As a rule of thumb, R_{sh} must be $\geq 10^6\ \Omega\ \mathrm{cm}^2$ and exceed R_{s} by at least two orders of magnitude[100]. Further insights on the role of R_{sh} and the best method of its extraction, either from the slope of J–V curves in the dark[104] or under different irradiances[100,103,105], should be a matter of more research.

Further, plots of J_{SC} and V_{OC} under varying irradiances can be used to assess device quality. A high-quality device will see J_{SC} scale linearly with irradiance and V_{oc} by $(nkT)\ln(10)$ per decade of light intensity, where n is the diode ideality factor. Deviations from these trends indicate defects and determine operational efficiency ranges. IEC recommends measurements at a minimum of five illuminance levels from 5% to 110% of primary measurement illuminance (for example, 50 → 100 → 200 → 500 → 1,000 lx) (ref. 28).

Dark current analysis provides additional insight into minimizing recombination. Xu et al. suggest the ratio of photocurrent density at 200 lx to dark recombination current should exceed 10 for obtaining efficient devices[100]. Furthermore, the rectifying characteristics of the devices[100,106,107], that is, the ratio of dark current density at +1 V (J_{on}) and at −1 V (J_{off}) should be higher than 10^2.

Stability testing for indoor photovoltaics

Transitioning from the laboratory to commercial deployment requires the technology to maintain performance over the lifetime of the intended application. For outdoor PV, lifespan and degradation rates are key factors in calculating economic metrics such as the levelized cost of electricity, critical for commercial viability[108]. Similarly, these parameters strongly influence the economic feasibility and sustainability of iPV that is aiming to provide durable, maintenance-free light-powered IoT devices. iPV technology lacks dedicated stability standards, unlike outdoor PV with established IEC protocols[7,9] and ISOS guidelines[88,109]. As best practice, we recommend continuing to use the current ISOS protocols and IEC tests meant for outdoors. It is almost certain that the lifetimes will be even greater when the product operates indoors.

However, while IEC 61215 and ISOS require testing modules through extreme conditions (light soaking, thermal cycling, damp heat, UV exposure), iPV operates in milder indoor environments. Thus, the iPV field requires both IEC-style validation protocols and flexible ISOS-style testing tailored to indoor applications to ensure consistent and uniform international reporting. Here we provide four initial best practice stability base tests for iPV, inspired by ISOS-D, ISOS-L and ISOS-LC.

Light-soaking test at 1,000 lx (BPIM-L1k-B#): the main best practice for indoor devices. Considering that laboratories will have the capability to shine WLEDs at 50, 200 and 1,000 lx for spot measurements, the device should be light soaked at 1,000 lx (at this higher lux, degradation mechanisms are more observable) and periodically measured at 1,000 lx. Example: BPIM-L1k-B3 indicates both soaking and measurement at 1,000 lx using LED B-3.

Light soaking at higher lux (BPIM-L#k-B#-##lx): acceleration factors for light soaking are technology dependent. Therefore, the research community is expected to evaluate stability at different illuminance levels under WLED, including values exceeding 1,000 lx for accelerated ageing studies (for example, 10,000 lx). Ideally, periodic PV performance measurements should be conducted during the light-soaking test at the 'best practice' illuminance of 200 lx (associated label: BPIM-L10k-B3-200lx), but practical challenges may require measurement at the same illuminance as that of soaking. Example: BPIM-L10k-B3-10klx indicates both soaking and measurement at 10,000 lx using LED B-3.

Dark-storage test (BPIM-D-B#-###lx): devices stored in dark ambient conditions with performance measured under best practice guidelines at 200 lx (preferred). Example: under the BPIM-D-B3-200lx test, performance is gauged periodically under LED B-3 light at 200 lx.

Light–dark cycling (BPIM-LC1k-1:#-B#): light:dark duty cycles of 1:1 or 1:2 over a number of 24-hour periods, simulating typical indoor conditions, providing insights into degradation reversibility and recovery times. Example: BPIM-LC1k-1:1-B3 indicates 12 h:12 h cycles, using 1,000 lx, LED B-3 light for both soaking and the periodic measurement of the DUT.

These four stability tests are designed to monitor performance over time at a single illuminance (for example, 1,000 lx) for practical reasons. To enable a meaningful comparison, additional measurements at other illuminance levels (that is, 200 lx, and where possible, 50 lx) should be carried out at the end of the test sequence. This allows the device parameters measured after stability testing to be directly compared with those obtained at the beginning under the same range of conditions. This applies equally when IEC or ISOS protocols are employed, where 1 Sun is the standard during the tests. During the tests, devices should be maintained at their maximum power point (MPP) when feasible, or at open circuit as an alternative. Initial tests can be carried out at ambient temperature, $T = (23 \pm 4)$ °C, and relative humidity (RH). T and RH must be reported and can be increased for accelerated studies in future. Statistical analysis is required on multiple devices under identical conditions with consistent fabrication and storage histories. Long experiments demand periodic monitoring of incident irradiance. When reporting normalized power or PCE versus time, the initial absolute value at the start of the test must be explicitly stated[110,111].

Given iPV's mild operating environment, the time required for efficiency to decay to 80% of initial values (t_{80}) may extend beyond practical experimental timeframes (10^3–10^4 h). Thus we recommend ageing the sample for a minimum of 1,000 hours if t_{80} is not reached and reporting the drop in PCE or MPD after this period[109]. Alternatively, elevated illuminance levels (1,000–20,000 lx) can accelerate degradation to achieve a practical t_{80} within ~1,000 hours. The t_{95} metric provides additional utility when t_{80} remains unrealized. Technologies may show transient effects such as burn-in (efficiency loss) and light-soaking (efficiency gain). Hartono et al. suggest tracking PCE change from the peak value, whereas for light cycling, energy yield combined with cycling ratio may be a preferable metric[110].

For the future, field testing is needed to create accelerated protocols that reliably predict iPV lifetime and degradation mechanisms under real operating conditions for each material technology[7–9]. Integration also requires compliance with electronic product standards, such as battery safety (IEC-62133, UL 2054) and RoHS regulations. Operational stability also can be affected by power management integrated circuits (ICs) through MPP tracking and disconnection cycles and operating in hybrid sun/indoor illumination (for example, near

 https://doi.org/10.1038/s41560-026-02101-x

Table 1 | Summary for best practices for indoor photovoltaic measurement (BPIM) regarding selection of the light source and preparation of the set-up for measurement of indoor PV devices

Item	Description	Recommendation level	Label	Comments
Light source (LS) type	WLED	Best practice	BPIM-B#-##lx	WLEDs are the most prevalent LS type for present and future. Use phosphor-converted WLEDs or hybrid RGBW LEDs.
	FL			
	User-defined (LS other than WLED/FL)			
Reference LED spectrum	LED B-4 (5,000 K)	Best practice	BPIM-B4-##lx	Current best practice as recommended by IEC TS 62607-7-2. Monitor future updates from IEC.
	LED B-3 (4,000 K)	Future best practice	BPIM-B3-##lx	Recommended for highest market applicability and matching CIE lighting calibration standards. We advocate the adoption of B-3 as reference for the future and consider it acceptable for measurements in the present due to small differences with respect to LED B-4. Labs should migrate to using this light source.
	LED B-1 (2,700 K)	Highly recommended (in addition to B.P. or for custom studies)	BPIM-B1-##lx	Recommended for residential areas
	LED B-2 (3,000 K)		BPIM-B2-##lx	Second best choice for residential areas
	LED B-5 (6,500 K)		BPIM-B5-##lx	Non-residential/industrial space and task lighting
Illuminance at the plane of the DUT	200 lx	Best practice	BPIM-B#-200lx	Commonly found in both residential and commercial areas
	1,000 lx	Highly recommended (in addition to B.P.)	BPIM-B#-1000lx	Found in well-lit commercial areas (for example, supermarkets)
	50 lx	Highly recommended (in addition to B.P.)	BPIM-B#-50lx	Found in less-lit horizontal walls and ceilings
Test enclosure	Light-tight enclosure	Best practice		Black opaque walls (reflectance <3–5%) with DUT holder and lamp holder
Illuminance adjustment system (IAS)	Illuminance controlled by power to LS (dimming)	Best practice	IAS-P	The range of achievable power levels can be limited. Some spectral shifts can occur with change in illuminance. Report spectral deviation if substantial.
	Illuminance controlled using optical media	Highly recommended	IAS-O	Some filters can result in considerable spectral shifts. Report spectral deviation if substantial.
	Illuminance controlled by distance	Third choice	IAS-D	Requires large volume. Spatial non-uniformity issues when LS comes close to DUT.
Method for classification of iPV measurement system	Spectral Coincidence (SC) Four methods available: SC_a, SC_b, SC_c, SC_d	SC_a Best practice	SA, A, B, C	Relative spectral irradiance of the reference and user-defined spectrum along with spectral responsivity or EQE of the DUT is required for calculation of SC_a.
		SC_b Highly recommended		Relative spectral irradiance of the reference and user-defined spectrum is required for calculation of SC_b.
		SC_c Highly recommended		Relative spectral irradiance of the reference and user-defined spectrum along with spectral responsivity or EQE of the DUT is required for calculation of SC_c.
		SC_d Third choice		Relative spectral irradiance of the reference and user-defined spectrum is required for calculation of SC_d.
	Temporal stability (TS) (one method only)	Best practice		Photometer or a photodiode can be used
	Spatial non-uniformity (SU) (one method only)	Best practice		Photometer or a photodiode can be used
Determination of illuminance and input irradiance (P_{in}) at DUT	Measure with a reference cell for reporting both MPD and PCE	Best practice		The reference cell must be calibrated. Spectral mismatch must be considered. Spectral and angular response should match that of DUT as closely as possible.
	Measure with calibrated spectroradiometer for reporting both MPD and PCE	Highly recommended		Calibrated or traceable to NMI. Dark spectrum must be subtracted before every measurement. Accuracy achieved for (quasi) collimated LS. For non-collimated LS, baffle plates must be used to reduce the effect of angular mismatch.
	Measure illuminance with calibrated luxmeter to report MPD. For reporting both MPD and PCE lamp spectrum must be known (either through spectroradiometers or provided by lamp maker)	Third choice (only for collimated light with calibrated instrumentation and with same spectrum used for measurement as that of calibration, that is, LED-B3)		Use luxmeters calibrated or traceable to NMI. Luxmeters must be of class AA as defined in JIS C 1609-1[123] or Class A as defined in ISO/CIE 19476[124] or DIN 5032-7[125]. Accuracy satisfactory only for spectra close to LED B-3 and for (quasi) collimated light at DUT.

The 'best practice' (B.P.) options are what we consider the first choice; also shown are the options that are highly recommended (as second choice) and the options that can be considered third choice. In the label column, we indicate the labels that can be reported when presenting data. For example, when measuring PV parameters under LED B-3 (with a CCT of 4,000 K) at an illuminance of 200 lx, one would use the label: BPIM-B3-200lx whereas BPIM-B4-1000lx would signify measurements were carried out under LED B-4 (CCT of 5,000 K) at an illuminance of 1,000 lx. FL, fluorescent lamp; JIS, Japanese Industrial Standards; DIN, Deutsches Institut für Normung; ISO, International Organization for Standardization.

Table 2 | Step-by-step checklist summarizing the best practices for indoor photovoltaic measurement (BPIM)

Step number	Task	Recommendation level	Report
(1)	Prepare measurement set-up	Best practice	Measurement set-up details listed in Table 1. iPV system classification
(2)	Select and switch on lamp and let light output stabilize (for example, wait 30 mins)	Best practice	Lamp type (either phosphor-converted WLEDs or hybrid RGBW WLEDs), make and model.
		Best practice	LED B-3 (4,000 K) as future or LED B-4 (5,000 K) as current best practices for widest applicability and benchmarking internationally
		Highly recommended (in addition to B.P.)	LED B-1 (2,700 K) where studies are focused on residential applications
		Highly recommended (in addition to B.P.)	Spectrum
(3)	Set illuminance using calibrated photometers	Best practice	200 lx (label: BPIM-B#-200lx)
		Highly recommended (in addition to B.P.)	1,000 lx (label: BPIM-B#-1000lx)
		Highly recommended (in addition to B.P.)	50 lx (label: BPIM-B#-50lx)
(4)	Determine the input irradiance (P_{in}) at DUT (for estimating PCE)	Highly recommended	P_{in} (using calibrated photometers), absolute $E(\lambda)$
(5)	Define area of the DUT	Best practice	Area defined by mask for small-area cells
		Best practice	Active area of DUT for large-area cells
		Best practice	Designated area for modules
(6)	Perform I–V scan	Best practice	Scan parameters
(7)	Verify output power (MPD) of DUT is stable over measurement time and over forward and reverse scans ($\Delta P_{max}/P_{max\_avg} \leq 2\%$)	Best practice	$\Delta P_{max}/P_{max\_avg}$
(8)	Measure PV parameters	Best practice	Cells: J_{SC}, V_{OC}, FF, MPD, PCE (statistical data)
			Modules: I_{SC}, V_{OC}, V_{MPP}, FF, P_{max}, PCE (statistical data)
(9)	If $\Delta P_{max}/P_{max\_avg} > 2\%$, perform I–V scans in both forward and reverse condition	Highly recommended	V_{OC}, I_{SC} (J_{SC}), FF, MPD, PCE (statistical data) for both forward and reverse bias
		Highly recommended	Plot maximum power over time for at least 60 s for best or representative device. Report stabilized MPD (or PCE) (if it reaches a plateau)
(10)	Provide current–voltage curves of representative or best-performing DUT	Highly recommended	J–V (for cells) or P–V and I–V (for modules) curves for best or representative devices.
(11)	Check that measured J_{SC} does not surpass the calculated maximum limits J_{cal_max} provided in tabular format in Box 3	Best practice	If $J_{SC} > J_{cal\_max}$, then recalibrate system (for reporting absolute performance) or clearly highlight this discrepancy (only for comparative studies)
(12)	Calculate integrated J_{cal} (with EQE and indoor photon flux at correct illuminance) and compare with measured J_{SC}	Highly recommended	Provide relative difference between integrated and measured J_{SC} (verify it is compatible with class of PV system and below at least 15–20%)

We consider the 'best practice' (B.P.) option the first choice; other options include highly recommended (as second choice).

windows). Future work should quantify these switching effects under different illumination and power management conditions[112,113].

Checklist

To summarize key findings, outcomes and recommendations, this section presents tables and a figure schematic in checklist format, serving as a rapid and rigorous reference that consolidates the key procedures described earlier. Table 1 summarizes recommendations for best practices for indoor photovoltaic measurement (BPIM) regarding the system/equipment. Users should select a light source (WLEDs or RGBW LEDs) with a spectrum as close as possible to either LED B-3 (4,000 K) as 'future best practice' or CIE LED B-4 (5,000 K) as 'current best practice' and use the corresponding CIE tabulated spectrum as reference. For residential iPV applications, the warmer 2,700 K spectrum (LED B-1) may be preferred to match typical home lighting conditions ('highly recommended').

Indoor PV measurements should be conducted under 200 lx (best practice). Additional measurements at 1,000 lx and 50 lx can be reported for the best-performing devices. Setting illuminance requires calibrated instruments traceable to NMIs. Users should document their measurement system's classification based on light stability, uniformity and spectral coincidence.

Table 2 outlines the procedure for iPV measurement. First, verify stabilization of lamp output (that is, after a warm-up period), set desired illuminance and calculate the input irradiance. Report the iPV measurement set-up details, including lamp specification, iPV system classification (Fig. 5a) and absolute spectral irradiance graph. Precisely define the DUT area with masking for cells ≤1 cm^2, then perform I–V scans to extract key parameters (I_{SC}, V_{OC}, FF, P_{max}). Report PCE, MPD (P_{max}), J_{SC} (I_{SC}), V_{OC} and FF for single-laboratory cells (modules). PCE should be reported when input irradiance is available (Fig. 5b). For modules, reporting P_{max}, I_{SC}, V_{mpp}, and PCE at standardized illumination

https://doi.org/10.1038/s41560-026-02101-x

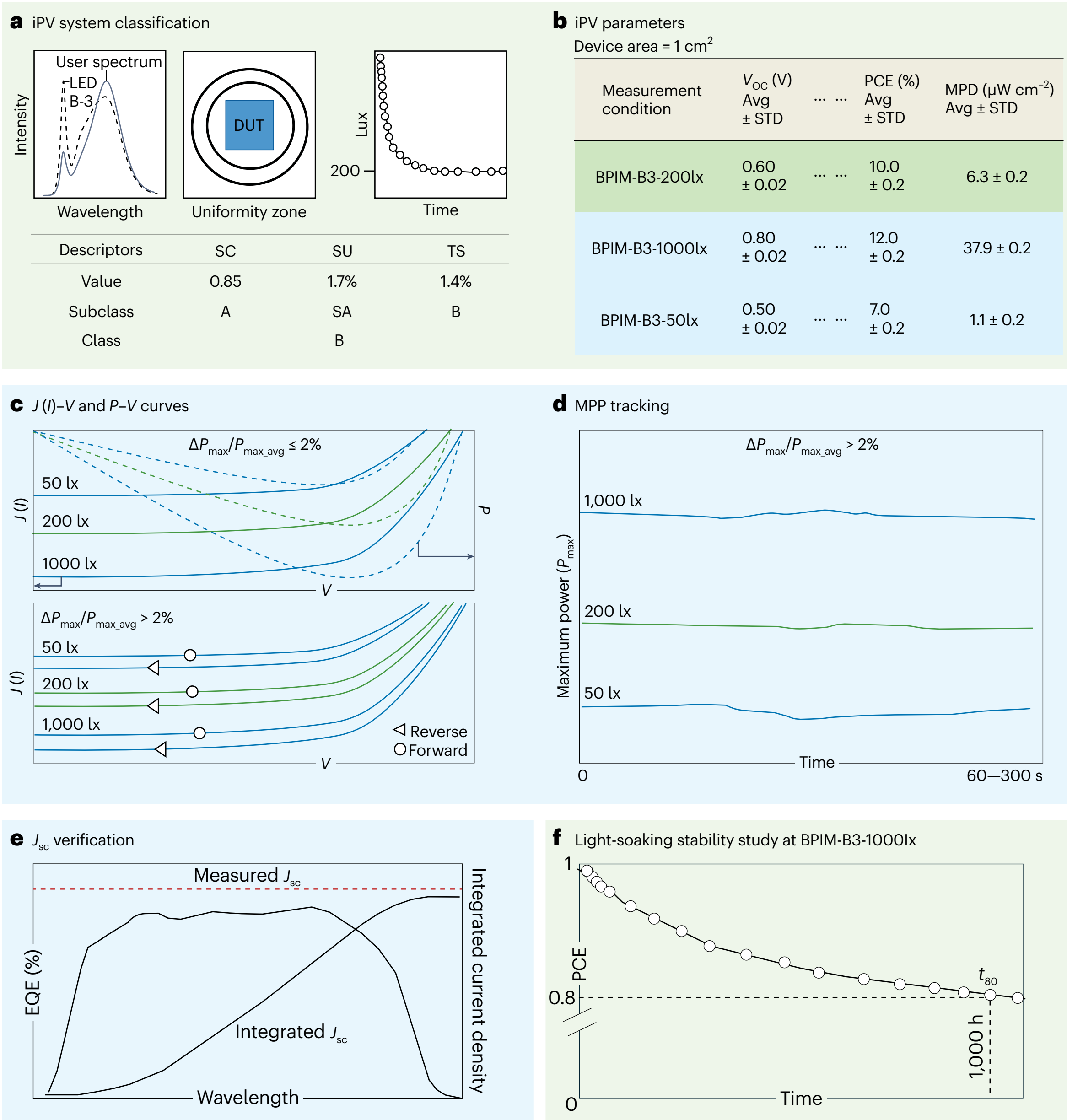

Fig. 5 | Illustrative examples on how to best report indoor photovoltaic device performance. **a**, iPV system classification showing, as an example, an LED spectral coincidence (SC) of 0.85 corresponding to class A, spatial non-uniformity (SU) of 1.7% corresponding to class SA and temporal stability (TS) of 1.4% corresponding to class B. The class of iPV system as a whole is B, defined by the lowest classification amongst the three descriptors. **b**, Reporting measured iPV parameters (average values with standard deviations) along with device area under BPIM measurement conditions at three illuminance levels BPIM-B3-(200, 1,000 and 50 lx), with 200 lx being the best practice (in green) and 1,000 lx and 50 lx highly recommended (in blue). Device area represents mask aperture area for small cells or designated area for modules. **c**, Representative current density–voltage (*J*–*V*) curves for small cells or current–voltage (*I*–*V*) curves for modules at multiple illuminance levels. Top: when maximum power variation $\Delta P_{max}/P_{max\_avg} \leq 2\%$, a single scan direction is sufficient; for modules, power–voltage (*P*–*V*) curves should also be plotted. Bottom: when $\Delta P_{max}/P_{max\_avg} > 2\%$, both forward and reverse scan directions must be reported to capture hysteresis behaviour. **d**, Alternative representation for unstable devices ($\Delta P_{max}/P_{max\_avg} > 2\%$): MPP tracking over 60–300 s showing temporal evolution of P_{max}, MPD or PCE at different illuminance levels. **e**, Verification through EQE measurement, comparing integrated current density, J_{cal}, with measured J_{SC} to ensure minimum current mismatch (typically within 10–20%). **f**, Long-term light-soaking stability study at BPIM-B3-1000lx showing PCE degradation over 1,000 hours with extraction of t_{80} (time to 80% of initial PCE). Figure not to scale (as indicated by the break mark in the *y* axis). Green-bordered panels (**a**,**b**,**f**) indicate mandatory reporting requirements; blue-bordered panels (**c**,**d**,**e**) represent highly recommended best practices for comprehensive device characterization.

levels (200, 1,000 and 50 lx) allows designers to match power, current, and voltage outputs with power management circuits and/or energy storage elements suited to the target application[31,97,114]. Power output of devices must remain stable during measurement ($\Delta P_{max}/P_{max\_avg} \leq 2\%$), otherwise, both forward and reverse sweep parameters and/or stabilized MPD/P_{max} (Fig. 5c,d) should be reported. For record-breaking cells, measurement accuracy is verified by ensuring experimental J_{SC} aligns within 10–20% of integrated J_{cal} (Fig. 5e) and does not exceed theoretical limits (Box 3). To simplify reporting, we recommend providing labels in the form BPIM-B#-##lx. For example, BPIM-B3-200lx signifies that the PV parameters were obtained for devices measured under LED B-3 light at 200 lx.

Table 3 reports recommendations regarding stability measurements. The current best practice is to follow the IEC or ISOS protocols,

 https://doi.org/10.1038/s41560-026-02101-x

Table 3 | Best practices for stability tests for indoor photovoltaic devices, arranged by priority level of best practice to third choice

	Stability test	Label	Recommendation level	Report
(1)	Use current IEC 61215 or ISOS protocols	Standard nomenclature established in the IEC or ISOS protocols.	Current best practice	Report the data required by IEC or ISOS protocols/tests for STC. Provide device performance not only at STC but also indoors (that is, under LED B-3 at 200 lx)
(2)	Light-soaking test at 1,000 lx also measured at 1,000 lx under LED B#	BPIM-L1k-B#	Best practice for indoors (testing at the 1,000 lx level corresponding to the upper lux of the three recommended values in Table 1)	Keep devices at MPP or open circuit. Provide performance at the same lux as light soaking, that is, 1,000 lx.
(3)	Light-soaking test under LED B#, soaking at XXX lx and measured at 200 lx or at the same XXX lx of light soaking.	BPIM-L#k-B#-##lx	Highly recommended (testing at higher indoor light-soaking levels, for example 10,000 lx) to determine, where possible, t_{80} and/or times to failure. Identify acceleration factors.)	Keep devices at MPP or open circuit. Provide performance at 200 lx or at the same lux as the continuous light-soaking conditions. Provide t_{80}
(4)	Dark-storage test	BPIM-D-B#-###lx	Highly recommended	Keep devices at open circuit. Provide performance at 200 lx
(5)	Light–dark cycling test at 1,000 lx	BPIM-LC1k-1:#-B#	Third choice These light-cycling tests are interesting for understanding operation in fluctuating environments mainly for academic/research purposes. For benchmarking the stability of devices, the continuous light-soaking tests should be used.	Keep devices at MPP or open circuit. Provide performance at the same lux as during the light-soaking cycle, that is, 1,000 lx. Report duty cycles (for example 1:1 or 1:2) even in the label. Cycling can also be operated under different illuminances.
(6)	All tests (1)–(5)	See above	Highly recommended	Measure PV performance at a single illuminance over the course of the tests; additional measurements at other lux levels should be taken at the end for comparison with initial values before the test.
(7)	All tests (1)–(5)	See above	Best practice	PCE (or MPD or P for modules) over time. Where normalized plots are shown, report initial PCE/MPD. Where applicable provide t_{80} (if within 1,000 h) or t_{95} drop after 10^3 hours where t_{80} is impractical. Tests at ambient temperature, $T = (23 \pm 4)$°C and ambient RH.

We consider the 'best practice' option the first choice; other options include highly recommended (as second choice) and the options that can be considered third choice. Each test specifies measurement conditions using designated LED B# (for example, B-3) sources and illuminance (###lx) levels (for example 200 lx or 1,000 lx). The labelling system follows the format BPIM-Test Type-B#-##lx, where BPIM stands for best practices for indoor photovoltaic Measurement, Test Type indicates the specific test (L1k for light soaking at 1,000 lx, D for Dark storage, LC1k for Light–Dark Cycling with light soaking at 1,000 lx), B# represents the specific LED spectrum used for illumination and ##lx represents the illuminance under which the measurement is done. For example, BPIM-L10k-B3-200lx specifies a light-soaking test with light soaking done at 10,000 lx (10k) under LED B-3, and the performance measurements are conducted at 200 lx illuminance.

which are meant for STC. For more specific tests related to indoors, we recommend light soaking (and measurement) at 1,000 lx (BPIM-L1k-B#) as the main best practice for indoors (Fig. 5f), then shelf-life testing in dark ambient conditions with periodic measurements at 200 lx (BPIM-D-B#-200lx) as highly recommended and light–dark cycling at 1000 lx (BPIM-LC1k-1:#-B#) as a third option. It is also 'highly recommended' to perform light soaking at higher illuminances (> 1,000 lx) to determine acceleration factors and to reach t_{80} values within a duration of 10^3 h. Tests should initially be conducted at ambient temperature (23 ± 4 °C) and relative humidity. Higher values can be adopted for studying acceleration factors in the future.

Conclusions

Indoor photovoltaic devices are emerging as sustainable energy solutions for IoT applications, yet inconsistent reporting methods necessitate standardization. Building on IEC specifications and laboratory experience, we recommend white LEDs matching the CIE LED B-3 spectrum (4,000 K) as the future standard, with LED B-1 (2,700 K) for residential-focused studies. PV parameters must be reported under 200 lx (supplemented by 1,000 lx and 50 lx for representative devices, where possible, for comprehensive characterization). We further provide best practices for measurement system set-up, classification, irradiance calibration, I–V measurements, parameter extraction and stability testing for indoor environments.

These best practices prioritize applicability, accuracy, repeatability and inter-laboratory uniformity. The complexity of some real-world scenarios (for example, PV near windows) may fall outside this guidance. Future work should continue to analyse best ways to tackle this complexity and system-level evaluation, including power management and energy storage integration, for real-world deployment. Regular reassessment will be necessary as photovoltaic and lighting technologies continue to evolve. Beyond inter-laboratory comparisons[22], establishing a global database would further enhance statistical reliability and accelerate progress. Finally, these measurement protocols also benefit related fields operating under indoor lighting, including energy harvesting[115,116], photodetection[117], indoor lighting[118], indoor visible light communications[119] and photovoltaic bioelectronics[120].

Methods

This work began with a group of authors carrying out initial studies and experiments to understand the intricacies of indoor PV measurement. The group expanded through coming together of researchers either aiming to prepare similar manuscripts or discussing this topic at (or in preparation for) various conferences including Materials Challenges in Alternative & Renewable Energy 2023 (MCARE 2023), Indoor Photovoltaics Conference 2024 (IPVC-1), PSMA International Energy Harvesting Workshop 2024 (EnerHarv2024), and Indoor Photovoltaics Conference 2025 (IPVC-2). Other researchers were invited to bring in device and application/system level expertise from different perspectives including from universities, research centres, industry, metrology institutions, panel experts working with standardization bodies and for a more comprehensive input on geography (for example, different lighting regulations) and applications (for example, developers of different technologies for photovoltaics, both established and start-ups, integrated circuits with which iPV is integrated, equipment manufacturers including measurement systems). Several draft versions of the manuscript were circulated among all authors until consensus was achieved. In cases where differing views persisted, recommendations were retained as optional to account for variations in laboratory capabilities, ensuring that comparable device performance reporting remains possible even without access to advanced instrumentation.

Market analysis

For the market analysis presented in Fig. 1a–b, we considered two broad categories of indoor lighting: residential and commercial/industrial. For the residential sector, we performed web scraping from two major vendors. From Amazon.com, an initial set of 421 products was identified using the keywords 'LED light bulb', which was refined to 195 unique LED products after removing duplicates and non-LED sources. Products were weighted by consumer review counts, used here as a proxy for sales volume. From the GE Lighting catalogue, 152 products were analysed from 256 listings in lighting-focused families (HD Light, Sun Filled LED, Ultra Bright LED), after excluding duplicates, outdoor lighting and minor structural variants. For the commercial/industrial sector, we examined the catalogues of two major providers: Lithonia Lighting (814 products) and Signify Lighting (875 products). Whereas this approach does not directly capture sales volumes, it provides a robust snapshot of prevailing market preferences across both residential and industrial contexts.

Lighting regulatory analysis

Regulatory perspectives vary by region. In 2013, the National Standard for Lighting Design of Buildings by the Ministry of Housing and Urban–Rural Development of China gave general recommendations based on application (homes, restaurants, bars: CCT < 3,300 K; office, classroom, reading room, shopping mall, laboratory, control room: 3,300 K to ~5,300 K; processing workshop, place with high illumination: >5,300 K) (ref. 121). In the more recent 2024 update[43], it was recommended that the CCT should not be higher than 4,000 K in indoor rooms or places where people work or stay for a long time at night (whereas the CCT of outdoor lighting should not be higher than 5,000 K). In Australia, 2,700–3,000 K (also described as 'warm white') is used for relaxed, warm ambience; 4,000 K (also described as 'cool white') for 'alertness' in functional areas such as educational buildings, retail displays and offices; and 5,000 K (also described as 'daylight') for hospitals and commercial applications[44]. In Türkiye, lighting standards specify 2,700–3,000 K for residential/hospitality settings, 4,000 K for offices/schools and 5,000–6,500 K for industrial spaces[45,46]. Russia mandates 4,000 K for offices, 5,000 K for industrial, 4,000–5,000 K for classrooms and 3,500–5,000 K for hospitals[47]. The US Department of Energy, in preparation for its 19 April 2024, 'Energy Conservation Standards for general service lamps', indicates 4,000 K and 2,700 K as the two representative CCTs in the tables provided[41].

Illuminance measurement

Lux measurements (HT 309 luxmeter, HT Instruments) for the last bar of Fig. 2a were carried out in an office at night measuring 8.3 m × 5.6 m × 3.0 m, illuminated by 26 ceiling OSRAM L 18 W/840 LUMILUX Cool White (4,000 K) 1,350 lm lamps. Illuminance was measured across desks (horizontal, facing ceiling), the ceiling (horizontal, facing the floor) and on the walls (vertical) over 45 data points in total.

Masking

J–*V* measurement of perovskite solar cells (ITO/SnO_2/$CH(NH_2)_2PbI_3$/spiro-MeOTAD/Au) with device area 16 mm^2 were measured under 1,000 lx LED (~20 cm from lamp) with and without black masks of aperture area of 12.25 mm^2. The integrated J_{SC} was calculated using the device EQE and 1,000-lx LED spectrum.

Data availability

Source data for Figs. 2 and 4 and the figure in Box 1 are available via Figshare at https://doi.org/10.6084/m9.figshare.29183996 (ref. 122).

References

1. Freunek, M., Freunek, M. & Reindl, L. M. Maximum efficiencies of indoor photovoltaic devices. *IEEE J. Photovolt.* **3**, 59–64 (2013).
2. Burwell, G. et al. Wide-gap perovskites for indoor photovoltaics. *Sol. RRL* **8**, 2400180 (2024).
3. Chakraborty, A. et al. Photovoltaics for indoor energy harvesting. *Nano Energy* **128**, 109932 (2024).
4. Grandhi, G. K. et al. Lead-free perovskite-inspired semiconductors for indoor light-harvesting - the present and the future. *Chem. Commun.* **59**, 8616–8625 (2023).
5. Brügge, F. et al. State of IoT—spring 2023. *IoT Analytics* https://iot-analytics.com/number-connected-iot-devices/ (2023).
6. Harrop, P. Battery elimination in electronics and electrical engineering 2018–2028. *IDTechEx* https://www.idtechex.com/en/research-report/battery-elimination-in-electronics-and-electrical-engineering-2018-2028/550 (2017).
7. *IEC 61215-1:2021. Terrestrial Photovoltaic (PV) Modules - Design Qualification and Type Approval* (IEC, 2021).
8. *IEC 61215-2:2021. Terrestrial Photovoltaic (PV) Modules - Design Qualification and Type Approval - Part 2: Test Procedures* (IEC, 2021).
9. *IEC 61215-1-3:2021. Terrestrial Photovoltaic (PV) Modules - Design Qualification and Type Approval - Part 1-3: Special Requirements for Testing of Thin-film Amorphous Silicon Based Photovoltaic (PV) Modules* (IEC, 2021).
10. *IEC 60904-1:2020. Measurement of Photovoltaic Current–Voltage Characteristics* (IEC, 2020).
11. Mathews, I., King, P. J., Stafford, F. & Frizzell, R. Performance of III-V solar cells as indoor light energy harvesters. *IEEE J. Photovolt.* **6**, 230–235 (2016).
12. Li, Y., Grabham, N. J., Beeby, S. P. & Tudor, M. J. The effect of the type of illumination on the energy harvesting performance of solar cells. *Sol. Energy* **111**, 21–29 (2015).
13. Chen, C.-Y. et al. Performance characterization of dye-sensitized photovoltaics under indoor lighting. *J. Phys. Chem. Lett.* **8**, 1824–1830 (2017).
14. Hoye et al. Reaching a consensus on indoor photovoltaics testing. *Joule* **9**, 102127 (2025).
15. Hamadani, B. H. & Campanelli, M. B. Photovoltaic characterization under artificial low irradiance conditions using reference solar cells. *IEEE J. Photovolt.* **10**, 1119–1125 (2020).
16. Cui, Y. et al. Accurate photovoltaic measurement of organic cells for indoor applications. *Joule* **5**, 1016–1023 (2021).
17. Lübke, D., Hartnagel, P., Angona, J. & Kirchartz, T. Comparing and quantifying indoor performance of organic solar cells. *Adv. Energy Mater.* **11**, 2101474 (2021).
18. Zeiske, S., Meredith, P., Armin, A. & Burwell, G. Importance of spectrally invariant broadband attenuation of light in indoor photovoltaic characterization. *APL Energy* **1**, 26103 (2023).
19. De Rossi, F., Pontecorvo, T. & Brown, T. M. Characterization of photovoltaic devices for indoor light harvesting and customization of flexible dye solar cells to deliver superior efficiency under artificial lighting. *Appl. Energy* **156**, 413–422 (2015).
20. Jailani, J. M. et al. Accurate performance characterization, reporting, and benchmarking for indoor photovoltaics. *Joule* https://doi.org/10.1016/J.JOULE.2025.102126 (2025).
21. Li-Kao, Z. J. et al. The dilemma of standardizing indoor photovoltaic characterisation: embracing diversity for powering the IoT. Preprint at https://arxiv.org/abs/2402.06630 (2024).
22. Eghbali, A. et al. Results of an international comparison of indoor photovoltaic measurements among seven metrological institutes. *Sol. RRL* **9**, 2400855 (2025).

23. Khambunkoed, N., Chen, C., Yuan, J.-R., Huang, H.-B. & Pecunia, V. Toward reliable characterization of nano-enabled indoor photovoltaics: accounting for device-dependent errors. *Nano Furtures* **10**, 015001 (2026).
24. Khampa, W. et al. A universal design and benchmarking framework for indoor photovoltaics. *Newton* **0**, 100437 (2026).
25. Radauer, A. Driving from the fringe into spotlight. The underrated role of standards and standardisation in RTDI policy and evaluation. *fteval J. Res. Technol. Policy Eval.* **51**, 59 (2020).
26. Pīlēna, A., Mežinska, I. & Lapiņa, I. Standardization as a catalyst for open and responsible innovation. *J. Open Innov. Technol. Mark. Complex.* **7**, 187 (2021).
27. Blind, K. *Standardisation as a Catalyst for Innovation. ERIM Report Series Reference No. EIA-2009-LIS* Vol. 253 (Springer, 1990).
28. *IEC TS 62607-7-2. Nanomanufacturing – Key control characteristics – Part 7-2: Nano-enabled photovoltaics – Device evaluation method for indoor light* (IEC, 2023).
29. Grandhi, G. K. et al. Promises and challenges of indoor photovoltaics. *Nat. Rev. Clean Technol.* **2025**, 1–16 (2025).
30. Blakesley, J. C. et al. Roadmap on established and emerging photovoltaics for sustainable energy conversion. *J. Phys. Energy* **6**, 041501 (2024).
31. Fleming, L. et al. Light powered battery-less non-dispersive infrared sensor for methane gas detection. In *Proc. SPIE 12999, Optical Sensing and Detection VIII, 129990LF* https://doi.org/10.1117/12.3022146 (2024).
32. Mathews, I., Kantareddy, S. N., Buonassisi, T. & Peters, I. M. Technology and market perspective for indoor photovoltaic cells. *Joule* **3**, 1415–1426 (2019).
33. Grandhi, G. K. et al. Underexplored dimensions of emerging indoor photovoltaics. *ACS Energy Lett.* **11**, 2474–2490 (2026).
34. Kokka, A. et al. Development of white LED illuminants for colorimetry and recommendation of white LED reference spectrum for photometry. *Metrologia* **55**, 526 (2018).
35. Elliott, C. & Lee, K. *Adoption of Light-Emitting Diodes in Common Lighting Applications* (U.S. Department of Energy, 2020).
36. LED light bulbs. *Amazon.com* https://go.nature.com/4wJtcyi (accessed 23 September 2025).
37. The leader in LED lighting solutions. *GE Lighting* https://www.gelighting.com/ (accessed 23 September 2025).
38. The best products in Europe. *Topten.eu* https://www.topten.eu/private (accessed 12 July 2024).
39. Best value in lighting. *Lithonia Lighting* https://lithonia.acuitybrands.com/ (accessed 8 January 2025).
40. Home. *Signify Company* https://www.signify.com/global (accessed 8 January 2025).
41. *2020 U.S. Lighting Market Characterization* (U.S. Department of Energy, 2024).
42. Office of Energy Efficiency and Renewable Energy. *Energy Conservation Program: Energy Conservation Standards for General Service Lamps, 10 CFR Part 430* (U.S. Department of Energy, 2023).
43. *GB/T 50034-2024 Standard for Lighting Design of Buildings* https://www.codeofchina.com/standard/GBT50034-2024.html (Chinese Standard, 2024).
44. *AS/NZS 1680.0:2009 Interior Lighting, Part 0: Safe Movement* https://store.standards.org.au/product/as-nzs-1680-0-2009 (Standards Australia, 2009).
45. *Light and Lighting - Basic Terms and Criteria for Specifying Lighting Requirements* TS EN 12665 https://intweb.tse.org.tr/standard/standard/Standard.aspx?0811180511151080511041191101040550471051021200881110431131040731011011210570660540900891000078102 (TSE, 2024).
46. *Light and Lighting - Lighting of Work Places - Part 1: Indoor Work Places* TS EN 12464-1 https://intweb.tse.org.tr/standard/standard/Standard.aspx?081118051115108051104119110104055047105102120088111043113104073084101104090050119097106118107122 (TSE, 2021).
47. SP 52.13330.2016 Daylighting and artificial lighting. https://www.russiangost.com/p-220763-sp-52133302016.aspx (Minstroy, 2016).
48. Poikonen, T. et al. *LED Reference Spectrum for Photometer Calibration* https://doi.org/10.25039/TR.251.2023 (International Commission on Illumination, 2022).
49. Brenes, R., Laitz, M., Jean, J., Dequilettes, D. W. & Bulović, V. Benefit from photon recycling at the maximum-power point of state-of-the-art perovskite solar cells. *Phys. Rev. Appl.* **12**, 014017 (2019).
50. Sun, C. C. et al. Packaging efficiency in phosphor-converted white LEDs and its impact to the limit of luminous efficacy. *J. Solid State Light.* **1**, 19 (2014).
51. Kusuma, P., Pattison, P. M. & Bugbee, B. From physics to fixtures to food: current and potential LED efficacy. *Hortic. Res.* **7**, 56 (2020).
52. Meyer-Arendt, J. R. Radiometry and photometry: units and conversion factors. *Appl. Opt.* **7**, 2081 (1968).
53. *EN 12464-1:2021 Light and Lighting 120* (European Standards Institution, 2021).
54. Seunarine, K. et al. Light power resource availability for energy harvesting photovoltaics for self-powered IoT. *J. Phys. Energy* **6**, 015018 (2024).
55. Solar cells. *TDK* https://product.tdk.com/en/search/solar-cell/catalog (accessed 6 February 2025).
56. Indoor PV components. *Lightricity* https://lightricity.co.uk/indoor-pv-components (accessed 6 February 2025).
57. Explore the world of indoor solar cells. *Epishine* https://www.epishine.com/solution/product (accessed 6 February 2025).
58. Solaires au silicium. *Solems.com* https://www.solems.com/en/indoor-solar-cells (accessed 6 February 2025).
59. OEM solar cell. *WSL Solar* https://www.wsl-solar.com/Oem_solar_panels (accessed 6 February 2025).
60. Powerfoyle. *Exeger* https://www.exeger.com/powerfoyle/ (accessed 6 February 2025).
61. Launch of thin dye-sensitized solar cell module panels - expanded product lineup enables various IoT devices to eliminate the need for battery replacement. *Fujikura* https://www.fujikura.co.jp/en/news/pressrelease/20200727_iot.html (2020).
62. Solid-state dye-sensitized solar cell. *Ricoh* https://www.ricoh.com/technology/tech/066_dssc (accessed 6 February 2025).
63. Amorton for the indoor environment. *Panasonic* https://industry.panasonic.eu/products/energy-building/amorphous-solar-cells/amorton-indoor-environment (accessed 6 February 2025).
64. Engineered solar products. *PowerFilm* https://www.powerfilmsolar.com/productsPowerFilm (accessed 6 February 2025).
65. Our technology. *Halocell Energy* https://www.halocell.energy/technology (accessed 6 February 2025).
66. Our products. *Saule Technologies* https://sauletech.com/product/ (accessed 6 February 2025).
67. Indoor DSSC technology. *G-LYTE* https://telecomreseller.com/2025/01/06/g-lyte-to-unveil-gold-standard-indoor-photovoltaic-solution-designed-to-power-billions-of-iot-devices-at-ces-2025/ (accessed 6 February 2025).
68. Technology - ambient photonics https://atmosic.com/partners/ambient-photonics/ (accessed 3 June 2024).
69. Indoor photovoltaics: the future of indoor solar panels. *Ossila* https://www.ossila.com/pages/indoor-photovoltaics-indoor-solar-panels (accessed 6 February 2025).
70. Shore, A. M. & Hamadani, B. H. Angular mismatch factor for reference cells under indoor light. In *Proc. 2024 IEEE 52nd Photovoltaic Specialist Conference (PVSC)* **307** (IEEE, 2024).

71. Huynh, M. Analyzing reflectance data for various black paints and coatings. In *Proc. Meeting Proceedings STO-MP-SET-277* 12-2–12-22 (NATO Science and Technology Organization, 2019).
72. Su, Z. et al. Designing LED array for uniform illumination distribution by simulated annealing algorithm. *Opt. Express* **20**, A843–A855 (2012).
73. Parsons, D. E., Koutsourakis, G. & Blakesley, J. C. Performance measurements for indoor photovoltaic devices: classification of a novel light source. *APL Energy* **2**, 16110 (2024).
74. *Photovoltaic Devices - Part 9: Classification of Solar Simulator Characteristics IEC 60904-9:2020* (IEC, 2020).
75. Habte, A. M. et al. *Developing a Framework for Reference Cell Standards for PV Resource Applications* (OSTI, 2018).
76. *IEC 60904-8:2014: Photovoltaic Devices - Part 8: Measurement of Spectral Responsivity of a Photovoltaic (PV) Device* (IEC, 2014).
77. Metzdorf, J. Calibration of solar cells 1: the differential spectral responsivity method. *Appl. Opt.* **26**, 1701 (1987).
78. Hamadani, B. H. & Roller, J. Reconciling LED and monochromator-based measurements of spectral responsivity in solar cells. *Appl. Opt.* **58**, 6173–6181 (2019).
79. Hamadani, B., Long, Y. S., Tsai, M. A. & Wu, T. C. Interlaboratory comparison of solar cell measurements under low indoor lighting conditions. *IEEE J. Photovolt.* **11**, 1430–1435 (2021).
80. *ASTM G138-12 Standard Test Method for Calibration of a Spectroradiometer Using a Standard Source of Irradiance* (ASTM, 2020).
81. Snaith, H. J. The perils of solar cell efficiency measurements. *Nat. Photon.* **6**, 337–340 (2012).
82. Ito, S. et al. Photovoltaic characterization of dye-sensitized solar cells: effect of device masking on conversion efficiency. *Prog. Photovolt. Res. Appl.* **14**, 589–601 (2006).
83. Snaith, H. J. How should you measure your excitonic solar cells? *Energy Environ. Sci.* **5**, 6513–6520 (2012).
84. Saliba, M. & Etgar, L. Current density mismatch in perovskite solar cells. *ACS Energy Lett.* **5**, 2886–2888 (2020).
85. Kiermasch, D., Gil-Escrig, L., Bolink, H. J. & Tvingstedt, K. Effects of masking on open-circuit voltage and fill factor in solar cells. *Joule* **3**, 16–26 (2019).
86. Tong, C. et al. Modeling the edge effect for measuring the performance of mesoscopic solar cells with shading masks. *J. Mater. Chem. A Mater.* **7**, 10942–10948 (2019).
87. How to improve measurement accuracy of LED and PV devices with a common electrode. *Fluxim* https://www.fluxim.com/measurement-accuracy-of-led-and-pv-devices-with-a-common-electrode (accessed 6 April 2025).
88. Reese, M. O. et al. Consensus stability testing protocols for organic photovoltaic materials and devices. *Sol. Energy Mater. Sol. Cells* **95**, 1253–1267 (2011).
89. *Measurement protocols for photovoltaic devices based on organic, dye-sensitized or perovskite materials*. IEC Technical Report 63228 (IEC, 2019).
90. Christians, J. A., Manser, J. S. & Kamat, P. V. Best practices in perovskite solar cell efficiency measurements. Avoiding the error of making bad cells look good. *J. Phys. Chem. Lett.* **6**, 852–857 (2015).
91. Zimmermann, E. et al. Characterization of perovskite solar cells: towards a reliable measurement protocol. *APL Mater.* **4**, 091901 (2016).
92. Rakocevic, L. et al. Reliable performance comparison of perovskite solar cells using optimized maximum power point tracking. *Sol. RRL* **3**, 1800287 (2019).
93. Pallares, R. M., Su, X., Lim, S. H. & Thanh, N. T. K. Fine-tuning of gold nanorod dimensions and plasmonic properties using the Hofmeister effects. *J. Mater. Chem. C Mater.* **4**, 53–61 (2015).
94. Pellet, N. et al. Hill climbing hysteresis of perovskite-based solar cells: a maximum power point tracking investigation. *Prog. Photovolt. Res. Appl.* **25**, 942–950 (2017).
95. Köbler, H. et al. High-throughput aging system for parallel maximum power point tracking of perovskite solar cells. *Energy Technol.* **10**, 2200234 (2022).
96. Meli, M. L. et al. Energy autonomous wireless sensing node working at 5 lux from a 4 cm^2 solar cell. *J. Low Power Electron. Appl.* **13**, 12 (2023).
97. Kauer, M. & Bellanger, M. in *Indoor Photovoltaics: Materials, Modeling and Applications* (ed. Freunek Müller, M.) 213–239 (John Wiley & Sons, 2020).
98. Ma, L. K. et al. High-efficiency indoor organic photovoltaics with a band-aligned interlayer. *Joule* **4**, 1486–1500 (2020).
99. Teran, A. S. et al. Energy harvesting for GaAs photovoltaics under low-flux indoor lighting conditions. *IEEE Trans. Electron Devices* **63**, 2820–2825 (2016).
100. Xu, J. et al. Key parameters and thresholds values for obtaining high performance perovskite solar cells indoors from full Br compositional and bandgap engineering. *ACS Appl. Energy Mater.* **6**, 10215–10224 (2023).
101. Chin, V. J., Salam, Z. & Ishaque, K. Cell modelling and model parameters estimation techniques for photovoltaic simulator application: A review. *Appl. Energy* **154**, 500–519 (2015).
102. Bader, S., Ma, X. & Oelmann, B. One-diode photovoltaic model parameters at indoor illumination levels – A comparison. *Sol. Energy* **180**, 707–716 (2019).
103. Müller, D. et al. Indoor Photovoltaics for the Internet-of-Things – A Comparison of State-of-the-Art Devices from Different Photovoltaic Technologies. *ACS Appl. Energy Mater.* **6**, 10404–10414 (2023).
104. Lübke, D., Hartnagel, P., Hülsbeck, M. & Kirchartz, T. Understanding the Thickness and Light-Intensity Dependent Performance of Green-Solvent Processed Organic Solar Cells. *ACS Mater. Au* **3**, 215–230 (2023).
105. Burwell, G. et al. Scaling Considerations for Organic Photovoltaics for Indoor Applications. *Sol. RRL* **6**, 2200315 (2022).
106. Lucarelli, G., Di Giacomo, F., Zardetto, V., Creatore, M. & Brown, T. M. Efficient light harvesting from flexible perovskite solar cells under indoor white light-emitting diode illumination. *Nano Res.* **10**, 2130–2145 (2017).
107. Dharmadasa, I. M., Rahaq, Y., Ojo, A. A. & Alanazi, T. I. Perovskite solar cells: a deep analysis using current–voltage and capacitance–voltage techniques. *J. Mater. Sci. Mater. Electron.* **30**, 1227–1235 (2019).
108. Peters, I. M., Hauch, J., Brabec, C. & Sinha, P. The value of stability in photovoltaics. *Joule* **5**, 3137–3153 (2021).
109. Khenkin, M. V. et al. Consensus statement for stability assessment and reporting for perovskite photovoltaics based on ISOS procedures. *Nat. Energy* **5**, 35–49 (2020).
110. Hartono, N. T. P. et al. Stability follows efficiency based on the analysis of a large perovskite solar cells ageing dataset. *Nat. Commun.* **14**, 1–7 (2023).
111. Zhu, H. et al. Long-term operating stability in perovskite photovoltaics. *Nat. Rev. Mater.* **8**, 569–586 (2023).
112. Jošt, M., Ajdič, Ž & Topič, M. Performance of triple-cation perovskite solar cells under different indoor operating conditions. *ACS Appl. Mater. Interfaces* **16**, 62195–62202 (2024).
113. Michaels, H. et al. Emerging indoor photovoltaics for self-powered and self-aware IoT towards sustainable energy management. *Chem. Sci.* **14**, 5350–5360 (2023).
114. Pirc, M., Ajdič, Ž, Uršič, D., Jošt, M. & Topič, M. Indoor energy harvesting with perovskite solar cells for IoT applications—a full year monitoring study. *ACS Appl. Energy Mater.* **7**, 565–575 (2024).
115. Pecunia, V. et al. Roadmap on energy harvesting materials. *J. Phys. Mater.* **6**, 042501 (2023).

116. Flores Diaz, N. et al. Unlocking high-performance photocapacitors for edge computing in low-light environments. *Energy Environ. Sci.* https://doi.org/10.1039/D5EE01052G (2025).
117. Morteza Najarian, A. et al. Photophysical properties of materials for high-speed photodetection. *Nat. Rev. Phys.* **6**, 219–230 (2024).
118. Boyce, P. R. Review: the impact of light in buildings on human health. *Indoor Built Environ.* **19**, 8–20 https://doi.org/10.1177/1420326X09358028 (2010).
119. Mapunda, G. A. et al. Indoor visible light communication: a tutorial and survey. *Wirel. Commun. Mob. Comput.* **2020**, 8881305 (2020).
120. Joseph, E. et al. Photovoltaic bioelectronics merging biology with new generation semiconductors and light in biophotovoltaics photobiomodulation and biosensing. *npj Biosens.* **1**, 1–44 (2024).
121. MOHURD & AQSIQ. *Standard for Lighting Design of Buildings GB 50034-2013* (Chinese Standard, 2013).
122. Chakraborty, A. Source data for 'best practices for measuring performance and stability of indoor photovoltaic devices'. *Figshare* https://doi.org/10.6084/m9.figshare.29183996 (2026).
123. *JIS C 1609-1:2006 Illuminance Meters Part 1: General Measuring Instruments* (Japanese Standards Association, 2006).
124. *ISO/CIE 19476:2014 - Characterization of the Performance of Illuminance Meters and Luminance Meters* (Commission Internationale de l´Eclairage, 2014).
125. *DIN 5032-7 Photometry - Part 7: Classification of Illuminance Meters and Luminance Meters* (Deutschen Institut für Normung, 2024).
126. Light sources. *European Commission* https://energy-efficient-products.ec.europa.eu/ecodesign-and-energy-label/product-list/light-sources_en (accessed 19 June 2024).
127. American Society for Testing and Materials (ASTM) G-173-03, reference air mass 1.5 spectra. *National Laboratory of the Rockies* https://www.nlr.gov/grid/solar-resource/spectra-am1.5 (2026).
128. CIE spectral luminous efficiency for photopic vision. *International Commission on Illumination* https://doi.org/10.25039/CIE.DS.dktna2s3 (2019).
129. EU Commission adopts regulation to ban all fluorescent lighting by September 2023. *ECEEE* https://www.eceee.org/all-news/news/eu-commission-adopts-regulation-to-ban-fluorescent-lighting-by-september-2023/ (2021).
130. *Fifth Meeting of the Conference of the Parties to the Minamata Convention on Mercury* (Conference of the Parties, 2023).
131. LED Basics. *U.S. Department of Energy* https://www.energy.gov/eere/ssl/led-basics (accessed 14 December 2024).
132. Revantino, Mangkuto, R. A., Suprijanto & Soelami, F. X. N. The impact of correlated colour temperature variation from a tuneable LED lamp on colour sample appearance shift in CIELAB colour space. *Optik* **267**, 169707 (2022).
133. Kazemi, R., Choobineh, A., Taheri, S. & Rastipishe, P. Comparing task performance, visual comfort and alertness under different lighting sources: an experimental study. *EXCLI J.* **17**, 1018 (2018).
134. Choudhury, A. K. R. in *Principles of Colour and Appearance Measurement* 1–52 (Woodhead Publishing, 2014).
135. Liu, C. et al. A review of subjective evaluation, physiological indicators and cognitive performance in indoor light environment: the role of illuminance and correlated color temperature. *J. Build. Eng.* **95**, 110224 (2024).
136. CIE 015:2018 colorimetry 4th edn. *International Commission on Illumination* https://doi.org/10.25039/TR.015.2018 (2018).
137. Relative spectral power distributions of illuminants representing typical LED lamps, 1 nm spacing. *International Commission on Illumination* https://doi.org/10.25039/CIE.DS.dhcw57sd (2018).
138. Almora, O. et al. Quantifying the absorption onset in the quantum efficiency of emerging photovoltaic devices. *Adv. Energy Mater.* **11**, 2100022 (2021).
139. Rau, U., Blank, B., Müller, T. C. M. & Kirchartz, T. Efficiency potential of photovoltaic materials and devices unveiled by detailed-balance analysis. *Phys. Rev. Appl.* **7**, 044016 (2017).

Acknowledgements

University of Rome Tor Vergata authors acknowledge funding from the European Union's Horizon Europe research and innovation programme under the Marie Skłodowska-Curie grant agreement number 101169056 (MENTOR), the Italian Ministry of University and Research (MUR) through the PRIN2022 PNRR INPOWER project number P2022PXS5S, PRIN2022 REPLACE (project number 2022C4YNP8), the Air Force Office of Scientific Research Biophysics Program (AFOSR award number FA9550-20-1-0157, FA9550-24-1-0320, FA9550-25-1-0361 and FA9550-26-1-0025) and the project IGEA-A0613- 2023-078007 and the Clean Energy Transition Partnership (CETP) under the 2022 CET Partnership joint call for research proposals, co-funded by the European Commission, grant agreement number 101069750 and the funding organizations detailed in https://cetpartnership.eu/funding-agencies-and-call-modules. T.M.B. gratefully acknowledges the European Commission and MUR Dual-Environment Perovskite Solar Cells: Powering Sustainable BIPV and IoT Integration (DEPSI) project under the framework of the CETP (EU project ID: CETP-FP-2024-00591, MUR code CETP-2024-TRANS-00119). A.C. acknowledges funding from the European Union's Horizon Europe research and innovation programme under the Marie Skłodowska-Curie grant agreement number 101111407 (PHOMOTRIPP) and Italian Ministry of University and Research (MUR) 'Funding projects presented by young researchers', Seal of Excellence (SOE) (project ID: 0000101). G.L. acknowledges the European Union's Horizon Europe research and innovation programme under grant agreement (PEARL project, number 101122283). G.G. acknowledges the European Research Council (ERC) under the European Union's Horizon Europe research and innovation programme ERC Cog 2024 ELOW-DI (grant agreement number 101171012). Funded by the European Union. Views and opinions expressed are, however, those of the authors only and do not necessarily reflect those of the European Union or ERCEA. Neither the European Union nor the granting authority can be held responsible for them. M.F. acknowledges the support by the Royal Society through the University Research Fellowship (URF/R1/191286), Research Grant 2021 (RGS/R1/211321) and United Kingdom Research and Innovation (UKRI) Engineering and Physical Sciences Research Council (EPSRC) Standard Grant EP/WO25280/1. M.L-C and Z.T. thank MCIN/AEI/10.13039/501100011033/FEDER, UE for the project PerMXSol, PID2022-143344OB-I00 and the PREP2022-000291 scholarship. To MICIU/AEI/10.13039/501100011033 for the project NextPVNet reference RED2024-154A8-T. G.B was supported by EPSRC through the Switch to Net Zero Buildings Place Based Impact Acceleration Account (reference EP/Y024060/1) and through the EPSRC Program Grant EP/T028511/1 Application Targeted Integrated Photovoltaics. G.K. acknowledges funding by the Department for Science, Innovation and Technology (UK) through the National Measurement System and the International Science Partnerships Fund (ISPF) project 'Setting the Standards for Semiconductors'. R.L.Z.H. thanks the UKRI for a Frontier Grant (EP/X022900/1), awarded through the 2021 ERC Starting Grant scheme, the Royal Academy of Engineering and Science and Technology Facilities Council for a Senior Research Fellowship (number RCSRF2324-18-68) and the Henry Royce Institute for an Industrial Collaborative Programme grant with Lightricity Ltd, funded by the EPSRC (EP/X527257/1). S.S. acknowledges financial support from the Department of Science & Technology (DST) Solar Challenge Award (DST/ETC/CASE/RES/2023/05(C)/(G)) and the Council of Scientific & Industrial Research-Fast Track Translation (CSIR-FTT) project (FTT 060511). P.V. thanks the Research Council of Finland, decision number 347772. The work is part of the Research Council of Finland Flagship Programme, Photonics Research and Innovation (PREIN), decision number 346511. M.J. and M.T. thank the Slovenian Research and Innovation Agency (ARIS), for funding programme P2-0415. A.D.C. acknowledges Enea contract /RdS25-27 - Progetto 1.5/. We also appreciate the efforts of PSMA's biennial EnerHarv workshop committees in 2024 and 2026 and the Horizon EU INFRACHIP Research Infrastructure (ID: 101131822) in helping us identify and connect with stakeholders to provide valuable inputs. T.M.B., A.C. and V.S. particularly acknowledge M. Costanza (Tyndall National Institute), L. Foelkel (Würth Elektronik), J. Hauch (Forschungszentrum Jülich), H. Kanaan (Dracula Technologies), T. Kaushalya (Nordic Semiconductor), R. La Rosa (STMicroelectronics), and J. Wright (jmachina.io) for useful discussions during the drafting of the manuscript and/or proofs. NIST disclaimer: certain commercial equipment, instruments, software or materials, commercial or non-commercial, are identified in this paper to specify the experimental procedure adequately. Such identification does not imply recommendation or endorsement of any product or service by NIST, nor does it imply that the materials or equipment identified are necessarily the best available for the purpose. We thank the International Electrotechnical Commission (IEC) for permission to reproduce information from its international standards (in particular, the Table in Fig. 3c). All such extracts are copyright of IEC, Geneva, Switzerland. All rights reserved. Further information on the IEC is available from www.iec.ch. IEC has no responsibility for the placement and context in which the extracts and contents are reproduced by the author, nor is IEC in any way responsible for the other content or accuracy therein.

Competing interests

F.D.G. is from Solertix, which develops perovskite-based PV modules. E.C. is from Halocell Europe, which also develops perovskite-based PV for indoor environments. D. Bagnis is from Oninn, which develops organic and perovskite-based PV modules. T.B. (senior staff) and S.K. (manager), both work in the Product Development and Engineering Division of Panasonic Solar Amorton Co., Ltd. D. Braga (sales and marketing) and A.C.V. (product manager) are from Fluxim AG, which commercializes measurement and simulation tools to assess the performance and stability of novel semiconductor devices. B.D. is the Marketing Director of e-peas, which develops and markets ultra-low power semiconductor technology. S.J. (point of contact and electronic integration manager) and F.S. (chief technical officer) are from G-Lyte, which manufactures dye-sensitized solar cell (DSSC)-based photovoltaic devices for indoor light harvesting. M.K. (chief executive officer) and A.Z. (research and development manager) are from Lightricity Ltd., which manufactures indoor and outdoor PV cells, indoor reference PV cells, a variety of PV-powered IoT sensors and indoor light simulators. R.L.Z.H. is chief technology officer of and holds financial interests in NanoPrint Innovations Ltd., which develops spatial atomic layer deposition systems for growing thin films for optoelectronics, including charge transport layers for photovoltaics. I.M. is the chief executive officer of Sensai Analytics, which uses artificial intelligence (AI) and data analytics to create 'Digital Twins' of electric vehicles. K. Wojciechowski at the moment of writing was a chief science officer in Saule S.A., which develops solar cells based on perovskite materials. M.I.S. is a co-founder of AY-Sensor Inc., which develops perovskite radiation detectors. The remaining authors declare no competing interests.

Additional information

Correspondence and requests for materials should be addressed to Thomas M. Brown.

Reprints and permissions information is available at www.nature.com/reprints.

Publisher's note Springer Nature remains neutral with regard to jurisdictional claims in published maps and institutional affiliations.

Abhisek Chakraborty[1], Giulia Lucarelli[1,2], Vaibhav Singh[1], Jie Xu[1,3], Zeynab Skafi[1], Diksha Thakur[1], Francesco Di Giacomo[4], Gyanendra Shankar[1], Emanuele Calabrò[5,6], Francesca De Rossi[1], Osbel Almora[7], Peyman Amiri[1], Shinji Aramaki[8], Diego Bagnis[9], Tomiki Bannai[10], Christoph J. Brabec[11,12,13], Daniele Braga[14], Gregory Burwell[15], Francesca Brunetti[1], Aldo Di Carlo[1,16], Matt Carnie[17], Luigi Angelo Castriotta[1], Sergio Castro-Hermosa[18], Manuela Ciocca[19], Yong Cui[20], Janardan Dagar[21], Bruno Damien[22], Sergey V. Dayneko[23], Nutifafa Y. Doumon[24,25], Vida Turkovic[26,27], Karen Forberich[12,13], Marina Freitag[28], Feng Gao[29], Giulia Grancini[30], Zhanglin Guo[31], Behrang Hamadani[32], Mike Hayes[33], Jianhui Hou[20,34], Robert L. Z. Hoye[35], Stéphane Jouin[36,37], Marko Jošt[38], Petri Kärhä[39], Matthias Kauer[40], Thomas Kirchartz[13,41], George Koutsourakis[42], Shuuji Kuge[10], Monica Lira-Cantu[43], Ian Mathews[44], Morten Madsen[26,27], Matthias Auf der Maur[1], Tsutomu Miyasaka[8], David Müller[45,46], Shashank Priya[47], Erin L. Ratcliff[48], Andrea Reale[1], Makhsud I. Saidaminov[23], Frédéric Sauvage[36,37], Suraj Soman[49,50], Zhenchuan Tian[43], Marko Topič[38], Antonio Cabas Vidani[14], Paola Vivo[51], Kai Wang[52,53], Yuming Wang[54], Zhao-Kui Wang[55], Konrad Wojciechowski[56,57], Uli Würfel[45,46,58], Xueqing Xu[59,60], Mustafa Yaşa[61], Selçuk Yerci[61,62], Andrea Zampetti[40], Kui Zhao[63] & Thomas M. Brown[1] ✉

[1]CHOSE (Centre for Hybrid and Organic Solar Energy), Department of Electronic Engineering, Tor Vergata University of Rome, Rome, Italy. [2]TNO, Solar Technologies & Applications, Eindhoven, The Netherlands. [3]School of Vehicle and Mobility, Tsinghua University, Beijing, China. [4]Solertix, Rome, Italy. [5]Halocell Europe, Rome, Italy. [6]Nuclear Department, ENEA C.R. Frascati, Frascati (RM), Italy. [7]Department of Electronic, Electric and Automatic Engineering, Universitat Rovira i Virgili, Tarragona, Spain. [8]Toin University of Yokohama, Yokohama, Japan. [9]PHD Semicon Research, SENAI FIEMG Innovation and Technology Center (CIT), Belo Horizonte, Brazil. [10]Panasonic Solar Amorton Co., Kitakata City, Japan. [11]Institute of Materials for Electronics and Energy Technology (i-MEET), Department of Materials Science and Engineering, Friedrich-Alexander-Universität Erlangen-Nürnberg (FAU), Erlangen,

Germany. [12]Helmholtz Institute Erlangen-Nürnberg for Renewable Energy (HI ERN), Erlangen, Germany. [13]IMD-3 Photovoltaics, Forschungszentrum Jülich GmbH, Jülich, Germany. [14]Fluxim AG, Winterthur, Switzerland. [15]Sustainable Advanced Materials (Sêr-SAM), Centre for Integrative Semiconductor Materials (CISM), Department of Physics, Faculty of Science and Engineering, Swansea University, Swansea, UK. [16]ISM-CNR, Istitute of Structure of Matter, Consiglio Nazionale delle Ricerche, Rome, Italy. [17]School of Engineering, Edith Cowan University, Joondalup, Australia. [18]GIIFET (Grupo de Investigación de las Ingenierías FET), Department of Electric Engineering, Fundación Escuela Tecnólogica de Neiva, Rivera, Colombia. [19]Faculty of Engineering, Free University of Bozen-Bolzano, Bolzano, BZ, Italy. [20]State Key Laboratory of Polymer Physics and Chemistry, Beijing National Laboratory for Molecular Sciences, Institute of Chemistry, Chinese Academy of Sciences, Beijing, China. [21]Helmholtz-Zentrum Berlin für Materialien (Solution-Processing of Hybrid Materials and Devices), Berlin, Germany. [22]e-peas, Louvain-La-Neuve, Belgium. [23]Department of Chemistry, University of Victoria, Victoria, British Columbia, Canada. [24]Department of Materials Science and Engineering, The Pennsylvania State University, University Park, PA, USA. [25]Department of Engineering Science and Mechanics, The Pennsylvania State University, University Park, PA, USA. [26]Centre for Advanced Photovoltaics and Thin Film Energy Devices (CAPE), Mads Clausen Institute, University of Southern Denmark, Sønderborg, Denmark. [27]SDU Climate Cluster, University of Southern Denmark, Odense, Denmark. [28]School of Natural and Environmental Science, Newcastle University, Newcastle, UK. [29]Department of Physics, Chemistry and Biology (IFM), Linköping University, Linköping, Sweden. [30]Department of Chemistry and INSTM, Università di Pavia, Pavia, Italy. [31]International Institute for Carbon-Neutral Energy Research (WPI-I2CNER), Kyushu University, Fukuoka, Japan. [32]National Institute of Standards and Technology, Gaithersburg, MD, USA. [33]Tyndall National Institute, Cork, Ireland. [34]University of Chinese Academy of Sciences, Beijing, China. [35]Inorganic Chemistry Laboratory, Department of Chemistry, University of Oxford, Oxford, UK. [36]Laboratoire de Réactivité et de Chimie des Solides, CNRS UMR7314, Université de Picardie Jules Verne, Hub de l'Energie, Amiens, France. [37]G-LYTE, Pont de Metz, France. [38]University of Ljubljana, Faculty of Electrical Engineering, Ljubljana, Slovenia. [39]Metrology Research Institute, Aalto University, Espoo, Finland. [40]Lightricity Ltd, Oxford, UK. [41]Faculty of Engineering and CENIDE, University of Duisburg-Essen, Duisburg, Germany. [42]National Physical Laboratory, Teddington, UK. [43]Catalan Institute of Nanoscience and Nanotechnology (ICN2), CSIC and The Barcelona Institute of Science and Technology, Universitat Autònoma de Barcelona, Bellaterra, Spain. [44]Sensai Analytics, Somerville, MA, USA. [45]Fraunhofer Institute for Solar Energy Systems ISE, Freiburg, Germany. [46]Freiburg Materials Research Center FMF, University of Freiburg, Freiburg, Germany. [47]Department of Chemical Engineering and Materials Science, University of Minnesota, Minneapolis, MN, USA. [48]School of Materials Science and Engineering, Georgia Institute of Technology, Atlanta, GA, USA. [49]Centre for Sustainable Energy Technologies (C-SET), CSIR-National Institute for Interdisciplinary Science and Technology (CSIR-NIIST), Thiruvananthapuram, India. [50]Academy of Scientific and Innovative Research (AcSIR), Ghaziabad, India. [51]Hybrid Solar Cells, Faculty of Engineering and Natural Sciences, Tampere University, Tampere, Finland. [52]Huanjiang Laboratory, Zhuji, China. [53]School of Aeronautics and Astronautics, Zhejiang University, Hangzhou, China. [54]The Materials and Electronics Research Center (MERC), School of Materials Science and Engineering, Changzhou University, Changzhou, China. [55]Institute of Functional Nano and Soft Materials (FUNSOM) Jiangsu Key Laboratory of Advanced Negative Carbon Technologies, Soochow University, Suzhuo, China. [56]Saule Technologies, Wrocław, Poland. [57]Saule Research Institute, Wrocław, Poland. [58]Cluster of Excellence livMatS, University of Freiburg, Freiburg, Germany. [59]School of Energy Science and Engineering, University of Science and Technology of China, Hefei, People's Republic of China. [60]Key Laboratory of Renewable Energy, Guangdong Provincial Key Laboratory of New and Renewable Energy Research and Development, Guangzhou Institute of Energy Conversion, Chinese Academy of Sciences, Guangzhou, People's Republic of China. [61]ODTÜ-GÜNAM, Middle East Technical University, Ankara, Türkiye. [62]Department of Electrical-Electronics Engineering, Middle East Technical University, Ankara, Türkiye. [63]Key Laboratory of Applied Surface and Colloid Chemistry, National Ministry of Education; Shaanxi Key Laboratory for Advanced Energy Devices, Shaanxi Engineering Lab for Advanced Energy Technology, School of Materials Science and Engineering, Shaanxi Normal University, Xi'an, China. ✉e-mail: thomas.brown@uniroma2.it